

RESEARCH

Open Access



Mn²⁺ modulates the expression of cellulase genes in *Trichoderma reesei* Rut-C30 via calcium signaling

Yumeng Chen, Yaling Shen, Wei Wang*  and Dongzhi Wei*

Abstract

Background: The filamentous fungus *Trichoderma reesei* Rut-C30 is one of the most vital fungi for the production of cellulases, which can be used for biofuel production from lignocellulose. Nevertheless, the mechanism of transmission of external stimuli and signals in modulating cellulase production in *T. reesei* Rut-C30 remains unclear. Calcium is a known second messenger regulating cellulase gene expression in *T. reesei*.

Results: In this study, we found that a biologically relevant extracellular Mn²⁺ concentration markedly stimulates cellulase production, total protein secretion, and the intracellular Mn²⁺ concentration of Rut-C30, a cellulase hyper-producing strain of *T. reesei*. Furthermore, we identified two Mn²⁺ transport proteins, designated as TPhO84-1 and TPhO84-2, indicating that they are upstream in the signaling pathway that leads to cellulase upregulation. We also found that Mn²⁺ induced a significant increase in cytosolic Ca²⁺ concentration, and that this increased cytosolic Ca²⁺ might be a key step in the Mn²⁺-mediated regulation of cellulase gene transcription and production. The utilization of LaCl₃ to block plasma membrane Ca²⁺ channels, and deletion of *crz1* (calcineurin-responsive zinc finger transcription factor 1) to interrupt calcium signaling, showed that Mn²⁺ exerts the induction of cellulase genes via calcium channels and calcium signaling. To substantiate this, we identified a Ca²⁺/Mn²⁺ P-type ATPase, TpmR1, which could play a pivotal role in Ca²⁺/Mn²⁺ homeostasis and Mn²⁺ induction of cellulase genes in *T. reesei* Rut-C30.

Conclusions: Taken together, our results revealed for the first time that Mn²⁺ stimulates cellulase production, and demonstrates that Mn²⁺ upregulates cellulase genes via calcium channels and calcium signaling. Our research also provides a direction to facilitate enhanced cellulase production by *T. reesei*.

Keywords: *Trichoderma reesei*, Mn²⁺ stimulation, Cellulase, Mn²⁺ transport, Calcium signaling, TpmR1

Background

Lignocellulosic biomass, the most abundant renewable energy source, can be hydrolyzed to sugars for bioethanol production. A common host cited for the production of cellulases and hemicellulases is the saprotrophic, filamentous fungus *Trichoderma reesei*, which is well known for its excellent ability to secrete a broad range of cellulases at very high levels [1–4]. Due to its ability to degrade and thrive on cellulose-containing fabrics, *T. reesei* has

attracted attention and was consequently studied in detail [5, 6]. However, compared with the energy-efficient production of cellulases and hemicellulases, the induction and regulation of the expression of genes encoding these enzymes in *T. reesei* are still not completely understood. Additionally, the induction of high-level cellulase production is dependent on inducers such as cellulose, D-xylose, lactose, or sophorose [3, 7–9], increasing the costs for the application of produced enzymes. Due to the extensive applications of cellulases and hemicellulases, the induction and regulation of the expression of genes encoding these enzymes have drawn significant attention.

Recent studies have demonstrated that cellulase production is regulated in response to environmental stress,

*Correspondence: wadexp@ecust.edu.cn; dzhwei@ecust.edu.cn
State Key Lab of Bioreactor Engineering, New World Institute of Biotechnology, East China University of Science and Technology, East China University of Science and Technology, 130 Meilong Road, P.O.B. 311, Shanghai 200237, China

such as light [10, 11], organic solvents [12], and metal ions [13–15]. A great example was shown by Chen and co-workers, who illustrated that Ca^{2+} plays an important role in the production of cellulase or hemicellulase in *T. reesei* Rut-C30 [13]. Chen et al. [13] suggested that external Ca^{2+} stimulated hyphal growth, growth-independent cellulase production, and total protein secretion of *T. reesei* Rut-C30 through the Ca^{2+} (calmodulin)–calcineurin–CRZ1 signal transduction pathway.

Intracellular accumulation of Mn^{2+} can interfere with calcium metabolism [16]. In *Ganoderma lucidum*, one of the most well-known medicinal basidiomycetes producing many bioactive compounds such as ganoderic acids, Mn^{2+} is thought to enhance cytosolic Ca^{2+} to induce ganoderic acid biosynthesis through the calcineurin signal pathway, to upregulate its biosynthetic genes at the transcriptional level [17]. In *Aspergillus nidulans*, high levels of Mn^{2+} can induce an increase in intracellular Ca^{2+} levels, which leads to the nuclear accumulation of CrzA [18, 19]. These observations suggest that Ca^{2+} and Mn^{2+} have relevant impacts on the cellular physiology and metabolism of various organisms.

The ability to sense and respond to Mn^{2+} by the production of import and efflux systems to maintain Mn^{2+} homeostasis is critical for cells [20–23]. Such homeostasis factors include cell surface and intracellular Mn^{2+} transporters that collectively guide the metal through a designated trafficking pathway [20, 22]. PMR1, a P-type ATPase ion pump, is a transporter for both Ca^{2+} and Mn^{2+} and is also a homeostasis factor, associating with delivering both Mn^{2+} and Ca^{2+} to the secretory pathway [22, 24–26]. Cytosolic Mn^{2+} accumulates in yeast cells lacking the PMR1 transporter [22]. Although many studies have reported on Mn^{2+} homeostasis in various organisms, the detailed mechanisms are yet unclear. First, studies have focused mainly on yeast or bacterial species, and less work has been conducted with filamentous fungi. Second, the detailed roles of Mn^{2+} in the biological processes of filamentous fungi remain unclear and need further studies. Third, the conjunction between Mn^{2+} and calcium signaling in filamentous fungi is still not clear. Therefore, it is necessary to study the mechanism of Mn^{2+} stimulation in filamentous fungi.

In this study, the impact of Mn^{2+} on the growth and protein production of *T. reesei* Rut-C30 was investigated. The temporal dynamics of intracellular and extracellular Mn^{2+} were detected. Additionally, the function of Mn^{2+} transport proteins in *T. reesei* Rut-C30 was characterized. The conjunction between Mn^{2+} and Ca^{2+} was further investigated to elucidate how Mn^{2+} regulates the production of cellulase via calcium signaling in *T. reesei* Rut-C30. These results could be used for more efficient production of cellulase by *T. reesei*, and provide a new approach to

understand the regulatory mechanisms that respond to environmental stimuli. This research may also offer the basis for the study of Mn^{2+} -induced signal transduction in other fungi.

Results

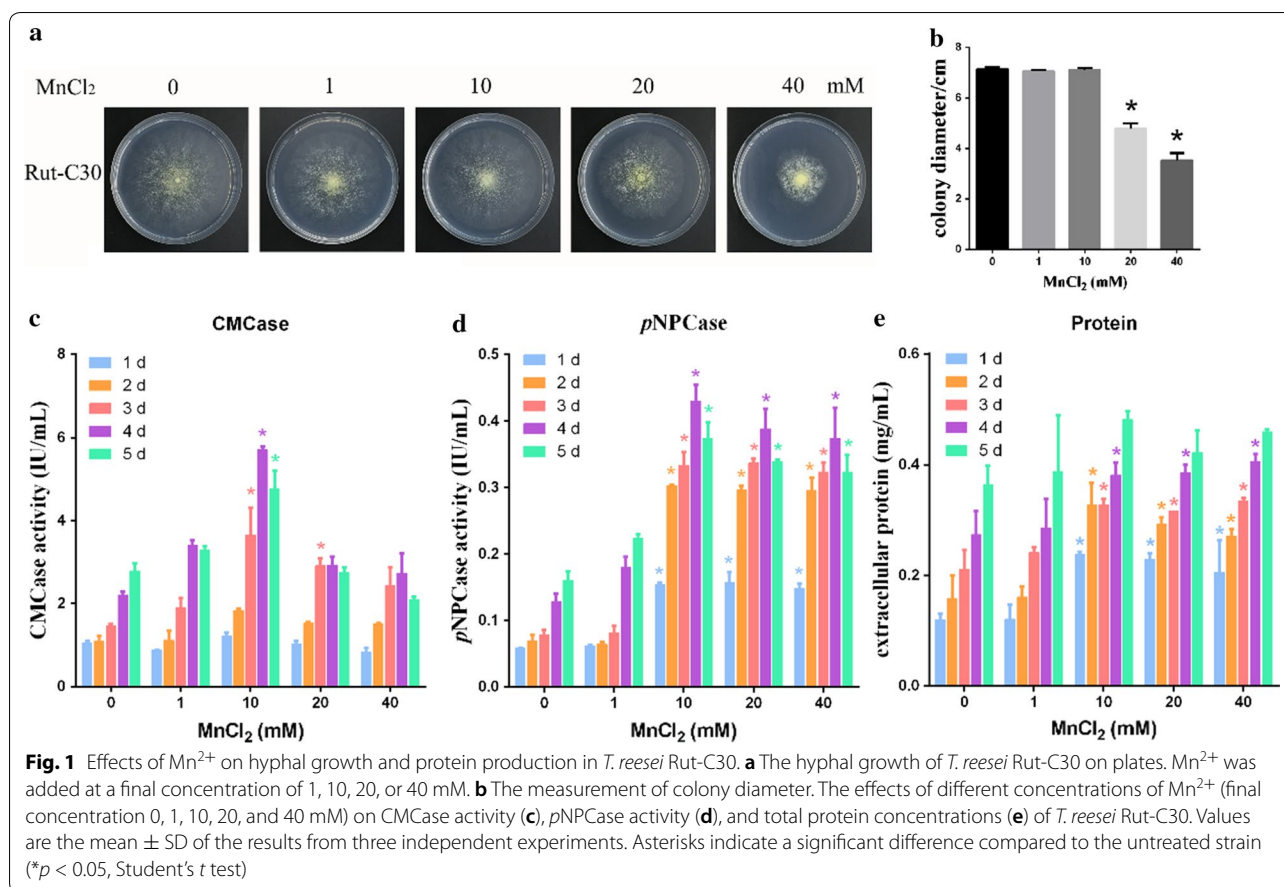
Effects of the addition of Mn^{2+} on growth and cellulase production of *T. reesei*

To determine how Mn^{2+} influences the hyphal growth, *T. reesei* Rut-C30 strains were cultured on MM (minimal medium) plates supplemented with different concentrations of Mn^{2+} (0, 1, 10, 20, and 40 mM final concentration) and 2% glucose as the sole carbon source. The mycelium length of *T. reesei* Rut-C30 after addition Mn^{2+} is shown in Fig. 1a. There was no significant difference in the hyphal growth with 1–10 mM Mn^{2+} . However, when the concentrations of Mn^{2+} increased to 20 mM, the strains grew more slowly and sparsely. As shown in Fig. 1b, treatment with 20 mM Mn^{2+} caused a 30% reduction in the colony diameter compared with that of the untreated strains. Moreover, after treatment with 40 mM Mn^{2+} , the treated strains showed a severe reduction in the colony diameter (53%).

To evaluate the effects of Mn^{2+} on cellulase production and total protein secretion, the same weight of precultured mycelia of *T. reesei* Rut-C30 was transferred to liquid MM containing 1% Avicel as the sole carbon source and different concentrations of Mn^{2+} (0, 1, 10, 20 and 40 mM). As shown in Fig. 1c (Additional file 8: Figure S7A), addition of Mn^{2+} at a final concentration of 10 mM significantly stimulated CMCase activity (representing *endo*- β -glucanase activity), with an increase of approximately 140% compared to the controls without addition of Mn^{2+} . However, 1, 20, and 40 mM of Mn^{2+} did not evidently affect CMCase activity. As shown in Fig. 1d (Additional file 8: Figure S7B) and e, the addition of Mn^{2+} at a final concentration of 10–40 mM significantly stimulated *pNPC*ase activity (representing *exo*- β -glucanase activity) and increased total protein concentration after 1 day of fermentation, with an increase of approximately 327 and 55%, respectively.

The above results demonstrated that 10–40 mM Mn^{2+} could stimulate cellulase production and total protein secretion in *T. reesei* Rut-C30, and that 20–40 mM Mn^{2+} could delay hyphal growth. The optimal concentration of Mn^{2+} to enhance cellulase production was 10 mM, which was selected for further research in our study. CMCase or *pNPC*ase activity was directly used to represent cellulase activity in our study.

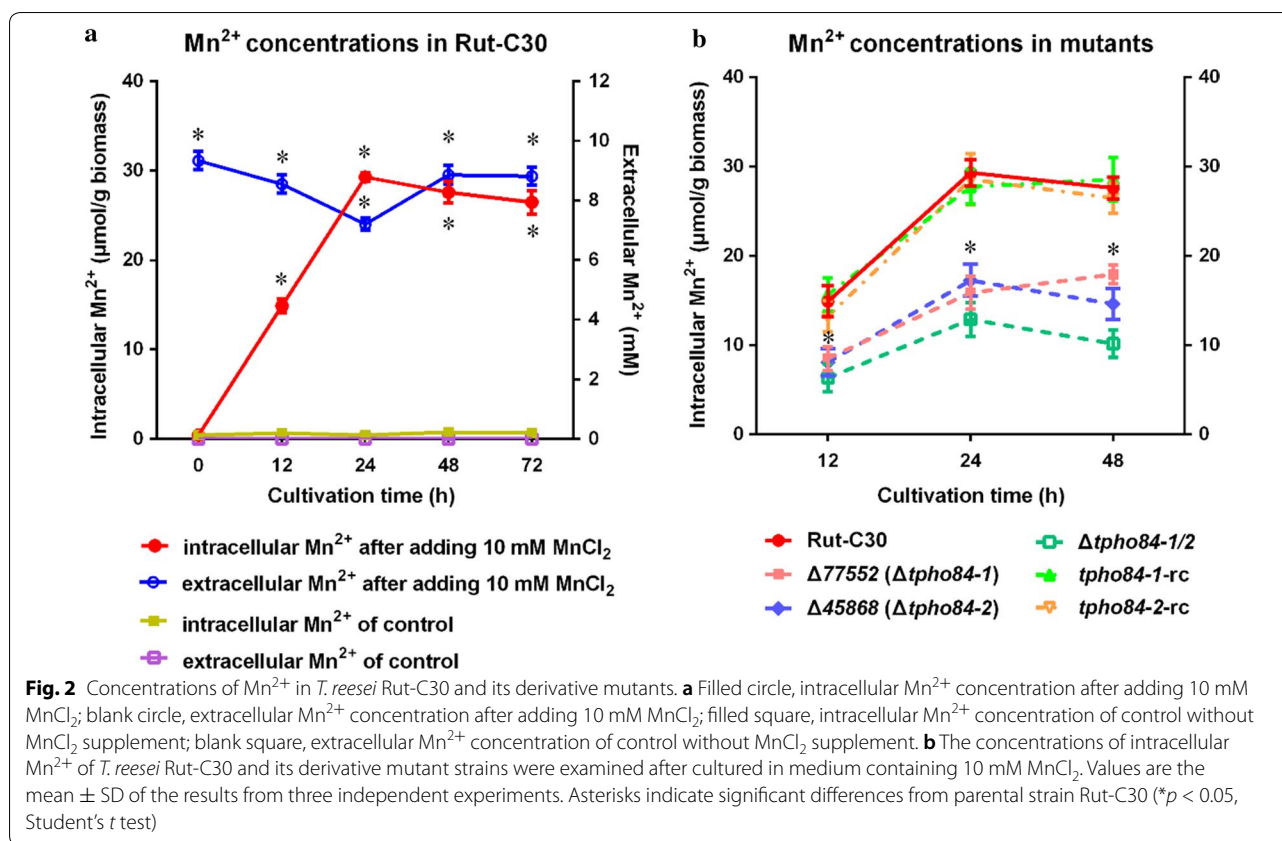
To further determine the effects of Mn^{2+} supplementation on the synthesis of cellulases or total protein secretion, the expression levels of four main cellulase genes (*cbh1* encoding cellobiohydrolase I, *cbh2* encoding cellobiohydrolase II, *egl1* encoding endoglucanase I, and *egl2*



encoding endoglucanase II), and a transcriptional regulator of cellulases, *xyr1*, were compared by quantitative reverse-transcription PCR (RT-qPCR) after induction for 24, 48, and 72 h in cultures with 0 or 10 mM Mn^{2+} supplementation. The primers used to detect transcriptional changes of these genes are listed in Additional file 1: Table S1. The transcriptional levels of four main cellulase genes significantly increased by almost 2- to 3.5-fold, after 24, 48, and 72 h of induction following supplementation with 10 mM Mn^{2+} (see Additional file 2: Figure S1A–D). In *T. reesei*, XYR1 is a global transcriptional activator of cellulose and hemicellulase genes [27]. In accordance with the transcription of *cbh1*, *cbh2* and *egl1*, *egl2*, the expression level of *xyr1* was also significantly stimulated after 72 h of induction (see Additional file 2: Figure S1E). These results were consistent with the upregulation of cellulase activity through the addition of 10 mM Mn^{2+} . However, when compared to expression of other cellulase-related genes, the delayed upregulation of *xyr1* expression implied that other putative regulators may participate in Mn^{2+} metabolism/regulation to directly induce cellulase gene expression, besides indirect induction through *xyr1*.

Variation in intracellular and extracellular Mn^{2+} concentration after the addition of Mn^{2+}

Extracellular Mn^{2+} can significantly augment the intracellular Mn^{2+} content, and subsequently affect the physiology and metabolism of *G. lucidum* [17]. To investigate whether enhanced cellulase production is linked to intracellular Mn^{2+} in *T. reesei* Rut-C30, the intracellular and extracellular Mn^{2+} concentrations were measured by inductively coupled plasma mass spectrometry (ICP-MS) during cultivation. As illustrated in Fig. 2a, the levels of intracellular and extracellular Mn^{2+} were almost constant in the control sample without Mn^{2+} addition. On the contrary, upon Mn^{2+} addition (10 mM final concentration), the intracellular Mn^{2+} concentration initially markedly increased, reaching its maximum at 24 h and then declined gradually, while the extracellular Mn^{2+} concentration dropped initially, reaching its minimum at 24 h and then increased gradually, suggesting that Mn^{2+} was transported into cells initially in response to a higher extracellular Mn^{2+} concentration. Subsequently, intracellular Mn^{2+} gradually effused into the medium from 24 h. We hypothesized that a mechanism could pump Mn^{2+} in and out of the cell.



Identification of Mn²⁺ transport proteins TPHO84-1 and TPHO84-2

Jensen et al. [16] suggested that PHO84, a low-affinity transporter of Mn²⁺ from *Saccharomyces cerevisiae*, transports Mn²⁺ when cells are exposed to higher Mn²⁺ concentrations. In our study, Mn²⁺ efficiently transported into *T. reesei* Rut-C30 cells at an Mn²⁺ concentration of 10 mM (Fig. 2a). To identify the protein(s) responsible for transporting Mn²⁺ in *T. reesei*, we conducted a homology search with the protein sequence of PHO84 (GenBank: KZV08715.1) in the *T. reesei* genome from the JGI database (<http://genome.jgi.doe.gov/Trire2/Trire2.home.html>). Five high score hits were obtained with the following protein identity matches: TRE77552, 59.6%, TRE81389, 51.8%, TRE45852, 49.0%, TRE45868, 40.1%, and TRE106118, 35.2%.

We hypothesized that Mn²⁺ transport proteins would be highly expressed during Mn²⁺ addition. To assess which proteins encoded putative Mn²⁺ transport activity, transcriptional levels of *tre77552*, *tre81389*, *tre45852*, *tre45868* and *tre106118* were monitored by RT-qPCR with 10 mM Mn²⁺ compared to no Mn²⁺ addition at different induction times. As illustrated in Additional file 3: Figure S2, expression of these genes was significantly upregulated in the samples treated with 10 mM Mn²⁺.

Based on their induction at higher Mn²⁺ concentration, all five genes might be responsible for Mn²⁺ transport of *T. reesei* Rut-C30.

To further investigate whether any of these five proteins displayed a function similar to that of PHO84, involved in transport of Mn²⁺ in *S. cerevisiae*, the five deletion mutants, Δ77552, Δ81389, Δ45852, Δ45868, and Δ106118, respectively, were collected to measure intracellular Mn²⁺ concentrations by ICP-MS compared to that in the parental strain. As shown in Fig. 2b, Δ77552 and Δ45868 showed a marked decrease in steady-state levels of cellular Mn²⁺ when compared with the Rut-C30 strain, in which a 70–80% decrease in metal accumulation was obtained. However, under the same conditions, Δ81389, Δ45852, or Δ106118 had an Mn²⁺ concentration similar to that in Rut-C30 strain (see Additional file 4: Figure S3). The *tre77552* and *tre45868* double mutant strain Δ*tpho84-1/2* showed lower intracellular Mn²⁺ concentration than each single mutant (Fig. 2b). Δ77552 and Δ45868 were also complemented by transforming vectors *ptpho84-1-rc* and *ptpho84-2-rc* into them, respectively (see Additional file 5: Figure S4). Complementation strains (*tpho84-1-rc* and *tpho84-2-rc*) were obtained to demonstrate the restoration of Mn²⁺ transport with intracellular Mn²⁺ concentrations similar to

those of the parent strain Rut-C30 (Fig. 2b). The results demonstrated that the intracellular Mn^{2+} concentration can be increased via putative Mn^{2+} transport proteins TRE77552 and TRE45868 in *T. reesei* Rut-C30.

As predicted by SMART (<http://smart.embl-heidelberg.de/>), both TRE77552 and TRE45868 are membrane proteins with an 11- and 9-transmembrane domain topology, respectively. To visualize the location of TRE77552 and TRE45868, we constructed two chimeric proteins, RFP-77552 and RFP-45868, by fusing red fluorescence protein to their N-terminus (see Additional file 6: Figure S5A). The two chimeric proteins were overexpressed via *cbh1* promoter, which allowed us to confirm that TRE77552 and TRE45868 are located at the mycelial surface. Additional file 6: Figure S5B shows the in vivo epifluorescence analysis of the two chimeric protein (RFP-77552 and RFP-45868) transformants, *rfp-tpho84-1* and *rfp-tpho84-2*, respectively, depicting strong and stable fluorescent signal at the mycelial surface, as expected for plasma membrane proteins. However, overexpression of genes encoding membrane bound proteins by a strong promoter might cause some uncertainty.

Based on these findings, we considered that both *tre77552* and *tre45868* encode Mn^{2+} transports with Mn^{2+} transport function located at the plasma membrane, and named the two genes as *tpho84-1* and *tpho84-2*, respectively. Intracellular Mn^{2+} can be transported into *T. reesei* Rut-C30 cells via TPHO84-1 and TPHO84-2. It is presently unclear whether *tre81389*, *tre45852*, and *tre106118* are inactive in the transport of Mn^{2+} .

Role of TPHO84-1 and TPHO84-2 in cellulase production

$\Delta 77552$ ($\Delta tpho84-1$) and $\Delta 45868$ ($\Delta tpho84-2$), and their complementation strains *tpho84-1-rc* and *tpho84-2-rc* were used to determine the effect of TPHO84-1 and TPHO84-2 in mediating the growth and cellulase production in *T. reesei* Rut-C30. To determine the effect of TPHO84-1 and TPHO84-2 on mediating growth, Rut-C30, $\Delta tpho84-1$, $\Delta tpho84-2$, *tpho84-1-rc*, *tpho84-2-rc* and $\Delta tpho84-1/2$ strains were cultured on minimal medium plates adding 0 or 10 mM Mn^{2+} and 2% glucose as the sole carbon source. The mycelium morphology is shown in Fig. 3a. There was no significant effect on the hyphal growth of Rut-C30, $\Delta tpho84-1$, $\Delta tpho84-2$, *tpho84-1-rc* and *tpho84-2-rc* strains at 0 or 10 mM Mn^{2+} . However, the hyphal growth of the $\Delta tpho84-1/2$ transformant was slightly repressed, compared with that of the parent strain at both 0 and 10 mM Mn^{2+} (Fig. 3b).

To further test the effect of Mn^{2+} transport proteins on cellulase production, we investigated the effect of Rut-C30, $\Delta tpho84-1$, $\Delta tpho84-2$, *tpho84-1-rc*, *tpho84-2-rc*, and $\Delta tpho84-1/2$ strains on cellulase production after supplementation of 0 or 10 mM Mn^{2+} . There was

no obvious difference in CMCCase (see Additional file 7: Figure S6A) and *pNPC*Case (see Additional file 7: Figure S6B) activities between these six strains without Mn^{2+} addition. However, $\Delta tpho84-1$ and $\Delta tpho84-2$ strains showed approximately 30–40% reduction in CMCCase activity, compared with the parental strain Rut-C30 with 10 mM Mn^{2+} addition. Furthermore, $\Delta tpho84-1/2$ strain had lower CMCCase activity than each single mutant, at approximately 50% reduction compared with Rut-C30 (Fig. 3c and Additional file 8: Figure S8A). Similarly, $\Delta tpho84-1$ and $\Delta tpho84-2$ strains showed approximately 25 to 30% reduction in the *pNPC*Case activity, compared with the parental strain Rut-C30, with 10 mM Mn^{2+} addition. Furthermore, the $\Delta tpho84-1/2$ strain showed lower *pNPC*Case activity than each single mutant, and approximately 40% reduction compared with Rut-C30 (Fig. 3d and Additional file 8: Figure S8B). The cellulase production capabilities of *tpho84-1-rc* and *tpho84-2-rc* were complemented at 10 mM Mn^{2+} supplementation compared to parental strains $\Delta tpho84-1$ and $\Delta tpho84-2$, respectively, to a level similar to that of the original strain Rut-C30 (Fig. 3c, d and Additional file 8: Figure S8A, B).

Additionally, RT-qPCR was performed to determine the transcription levels of the important cellulase genes *cbh1* and *egl1* in the *T. reesei* Rut-C30, $\Delta tpho84-1$, $\Delta tpho84-2$, *tpho84-1-rc*, *tpho84-2-rc*, and $\Delta tpho84-1/2$ mutants. The primers used to detect transcriptional levels of these genes are listed in Additional file 1: Table S1. In agreement with the CMCCase activity levels, no obvious difference in transcription levels of *cbh1* and *egl1* between above six strains was observed without Mn^{2+} addition (data not shown). However, the deletion strains $\Delta tpho84-1$, $\Delta tpho84-2$, and $\Delta tpho84-1/2$ showed a marked reduction in cellulase transcription compared with the parental strain Rut-C30 upon 10 mM Mn^{2+} addition at all time points examined (Fig. 3e, f). Similarly, the expression levels of the *cbh1* and *egl1* genes of *tpho84-1-rc* and *tpho84-2-rc* were complemented under Mn^{2+} supplementation, to a level similar to that of the original strain Rut-C30.

These results indicate that TPHO84-1 and TPHO84-2 participate in inducing cellulase production of *T. reesei* Rut-C30 only under Mn^{2+} addition, which is in accordance with its function as Mn^{2+} transport protein.

Increase in cytosolic Ca^{2+} level and calcium signaling after Mn^{2+} addition

Next, we investigated how Mn^{2+} addition can upregulate cellulase gene expression via Mn^{2+} transport proteins TPHO84-1 and TPHO84-2. Using Fluo-3/AM fluorescent dye, a dye that only emits green fluorescence after crossing the cell membrane and binding with Ca^{2+} [28], whose intensity represents relative amounts of free

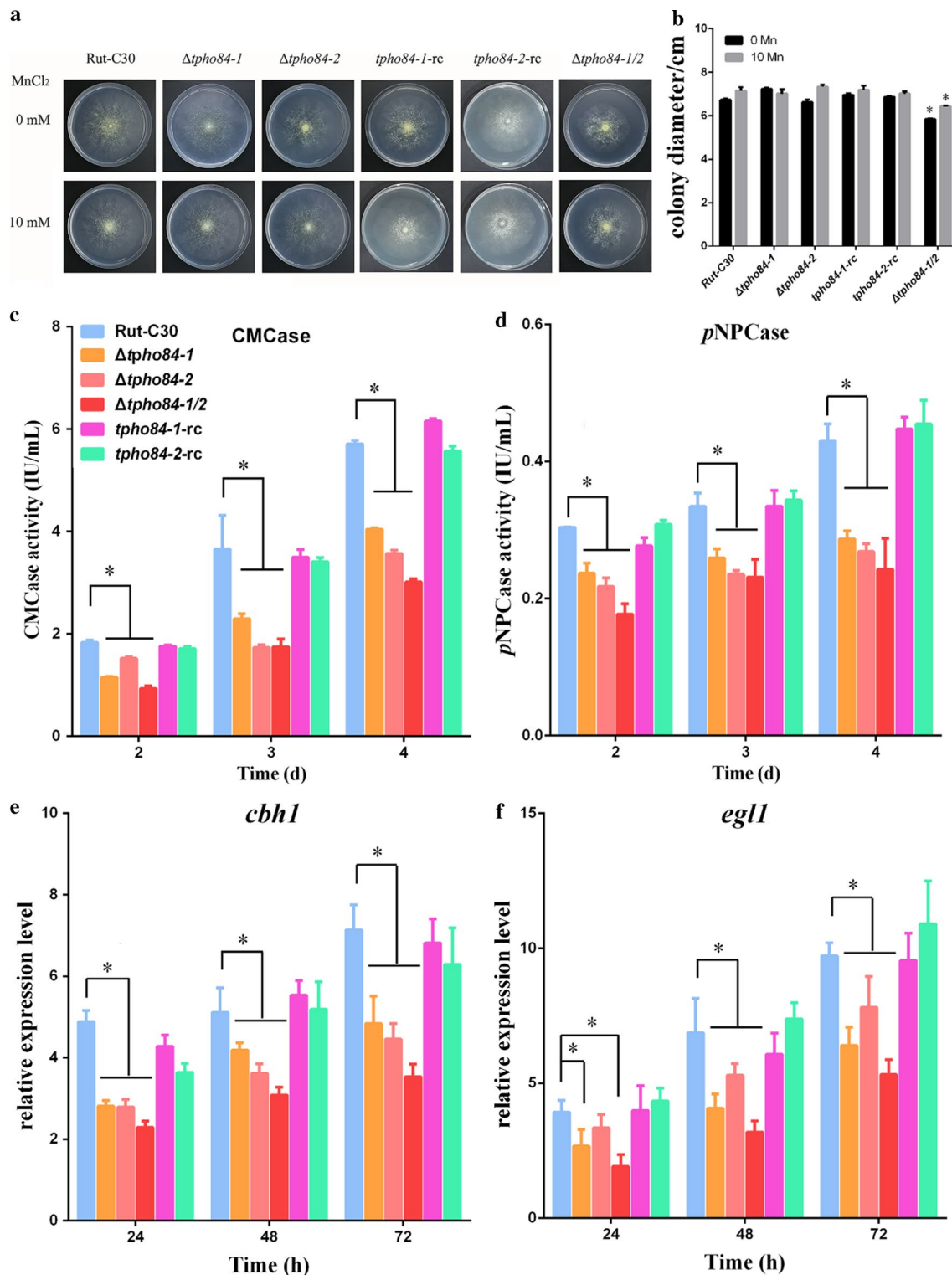


Fig. 3 TPHO84-1 and TPHO84-2 regulate cellulase production of *T. reesei* Rut-C30 with Mn²⁺ supplementation. **a** The hyphal growth of *T. reesei* Rut-C30 and its derivative mutant strains under 0 or 10 mM MnCl₂. **b** The measurement of colony diameter. The CMCase activity (**c**) and pNPCase activity (**d**) of *T. reesei* Rut-C30 and its derivative mutant strains were examined after culture in medium containing 0 or 10 mM MnCl₂. The transcriptional levels of *cbh1* (**e**) and *egl1* (**f**) in the parental strain Rut-C30 and its derivative mutant strains were analyzed after cultured in medium containing 0 or 10 mM MnCl₂. Values are the mean ± SD of the results from three independent experiments. Asterisks indicate significant differences (**p* < 0.05, Student's *t* test)

intracellular Ca^{2+} [29], we found that the cytosolic Ca^{2+} concentration was increased after Mn^{2+} addition. As shown in Fig. 4A, a stronger green fluorescence intensity was observed in the Rut-C30 cells under 10 mM Mn^{2+} supplement on the second day than that observed with the control (no Mn^{2+} supplement), demonstrating that Mn^{2+} leads to an increase in the level of cytosolic Ca^{2+} . The fluorescence level emitted by the Ca^{2+} -activated fluorochrome reached a 2.23-fold increase under 10 mM Mn^{2+} addition compared to that in the control (Fig. 4B). These results indicate that Mn^{2+} induced an increase in the concentration level of cytosolic Ca^{2+} . A similar phenomenon was reported in *S. cerevisiae* [30].

We measured the level of cytosolic Ca^{2+} in the $\Delta\text{tpho84-1}$, $\Delta\text{tpho84-2}$, and $\Delta\text{tpho84-1/2}$ strains with Mn^{2+} addition. As illustrated in Fig. 4A, B, the significant increase in intracellular Ca^{2+} induced by Mn^{2+} , observed in parental strain Rut-C30, was absent in the $\Delta\text{tpho84-1}$, $\Delta\text{tpho84-2}$, and $\Delta\text{tpho84-1/2}$ strains. The augmentation of cytosolic Ca^{2+} levels induced by Mn^{2+} was blocked in the $\Delta\text{tpho84-1}$, $\Delta\text{tpho84-2}$, and $\Delta\text{tpho84-1/2}$ strains. These results suggest that rising cytosolic Ca^{2+} levels depend on Mn^{2+} transport into Rut-C30 cells via TPHO84-1 and TPHO84-2. This also indicates that Ca^{2+} influx in cells is closely associated with Mn^{2+} homeostasis.

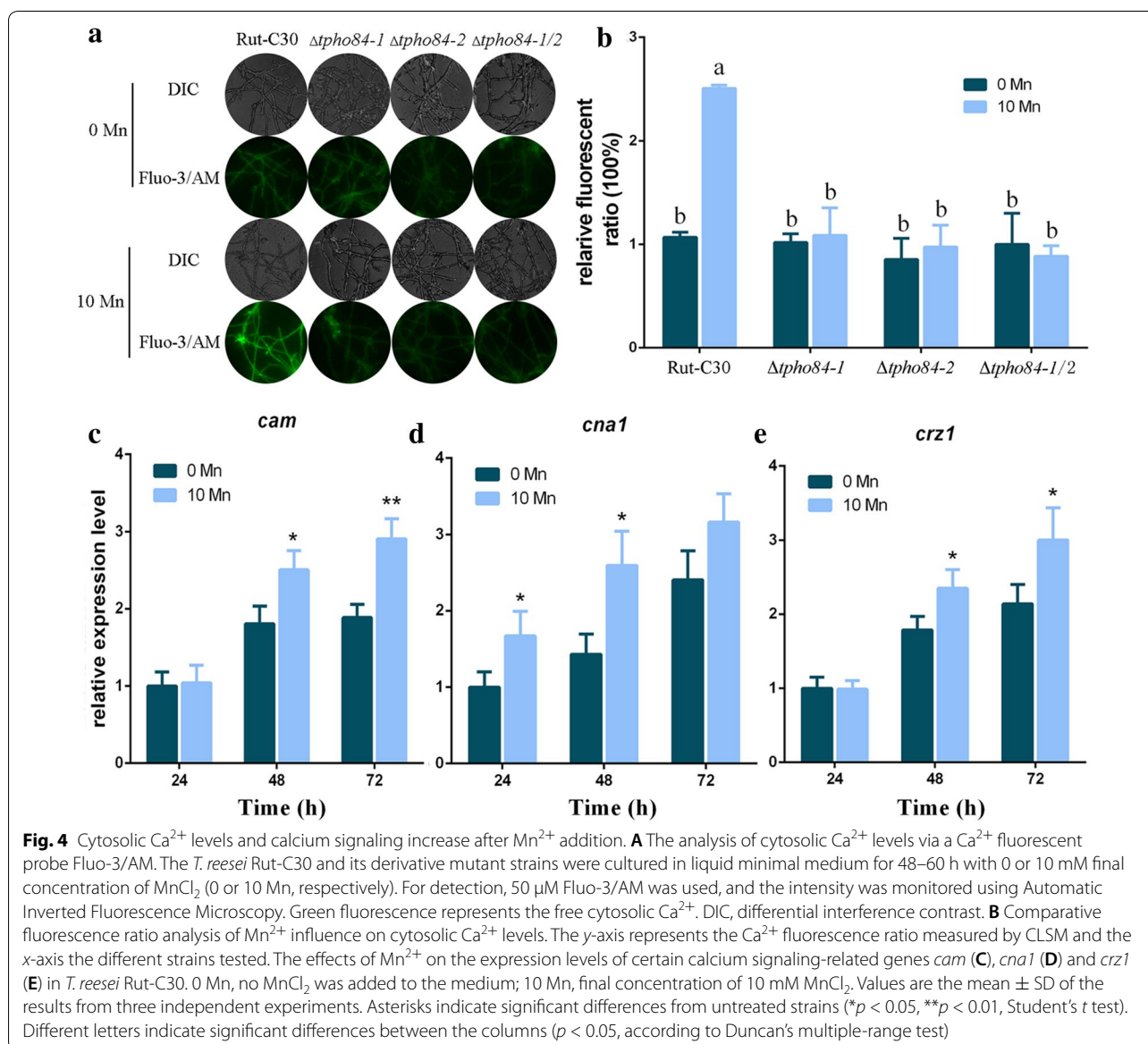


Fig. 4 Cytosolic Ca^{2+} levels and calcium signaling increase after Mn^{2+} addition. **A** The analysis of cytosolic Ca^{2+} levels via a Ca^{2+} fluorescent probe Fluo-3/AM. The *T. reesei* Rut-C30 and its derivative mutant strains were cultured in liquid minimal medium for 48–60 h with 0 or 10 mM final concentration of MnCl_2 (0 or 10 Mn, respectively). For detection, 50 μM Fluo-3/AM was used, and the intensity was monitored using Automatic Inverted Fluorescence Microscopy. Green fluorescence represents the free cytosolic Ca^{2+} . DIC, differential interference contrast. **B** Comparative fluorescence ratio analysis of Mn^{2+} influence on cytosolic Ca^{2+} levels. The y-axis represents the Ca^{2+} fluorescence ratio measured by CLSM and the x-axis the different strains tested. The effects of Mn^{2+} on the expression levels of certain calcium signaling-related genes *cam* (**C**), *cna1* (**D**) and *crz1* (**E**) in *T. reesei* Rut-C30. 0 Mn, no MnCl_2 was added to the medium; 10 Mn, final concentration of 10 mM MnCl_2 . Values are the mean \pm SD of the results from three independent experiments. Asterisks indicate significant differences from untreated strains (* $p < 0.05$, ** $p < 0.01$, Student's *t* test). Different letters indicate significant differences between the columns ($p < 0.05$, according to Duncan's multiple-range test)

Previous studies have demonstrated that the calcium signal transduction pathway can upregulate cellulase gene expression [13]. We investigated whether the increased levels of cytosolic Ca^{2+} , induced by Mn^{2+} , can trigger calcium signal transduction pathways in *T. reesei*. To test our hypothesis, RT-qPCR was carried out to analyze the transcriptional levels of calcium signaling-related genes, including calmodulin (*cam*, GenBank: ACZ26150.1), calcineurin (*cna1*, GenBank: EGR49476.1) [31], and calcineurin-responsive zinc finger transcription factor 1, *crz1* [13], under Mn^{2+} addition. The primers used to detect transcription of these genes are listed in Additional file 1: Table S1. As shown in Fig. 4C–E, similar to the increase in the contents of cytosolic Ca^{2+} , expression of these genes was significantly upregulated with Mn^{2+} addition. These results suggested that Mn^{2+} can increase the concentration of cytosolic Ca^{2+} , thus stimulating the calcium signal transduction pathway to induce cellulase production in *T. reesei* Rut-C30.

***Mn*²⁺ induces cellulase production via cytosolic *Ca*²⁺**

To investigate the assumption that Mn^{2+} induces cytosolic Ca^{2+} improvement and cellulase production via Ca^{2+} channels, we used LaCl_3 , a plasma membrane Ca^{2+} channel blocker to prevent influx of external Ca^{2+} [32]. Figure 5A, B shows that the Fluo-3/AM fluorescence intensity of mycelia remarkably reduced almost 60% with LaCl_3 compared with no LaCl_3 addition, under 10 mM Mn^{2+} . The increased content of cytosolic Ca^{2+} induced by Mn^{2+} could be effectively attenuated by adding LaCl_3 to *T. reesei* Rut-C30. Meanwhile, the increased expression of calcium signaling-related genes, *cam*, *cna1*, and *crz1*, which are induced by 10 mM Mn^{2+} , was also effectively prevented by adding LaCl_3 (data not shown).

Ca^{2+} participates in regulating cellulase production in *T. reesei* [13]. To investigate whether a cellulase increase, induced by Mn^{2+} , was blocked by LaCl_3 , we analyzed CMCase and *pNPC*ase activities and transcription of key cellulase genes *cbh1* and *egl1*. As shown in Fig. 5C, D (Additional file 8: Figure S9A, B), under Mn^{2+} supplementation and with LaCl_3 , the CMCase and *pNPC*ase

activities in *T. reesei* Rut-C30 decreased by 50 and 49%, respectively, compared with no LaCl_3 addition. Meanwhile, the expression levels of *cbh1* and *egl1* were reduced by 60% at 72 h (Fig. 5E, F). However, there was no obvious change to CMCase activities and transcriptional levels of *cbh1* and *egl1* with or without LaCl_3 when Mn^{2+} was not added (Fig. 5C–E, Additional file 8: Figure S9A, B). These results showed that LaCl_3 could significantly decrease the Mn^{2+} -induced high expression levels of key cellulase genes in *T. reesei* Rut-C30.

These data indicated that Mn^{2+} induced cytosolic Ca^{2+} increase via the Ca^{2+} channel. When a Ca^{2+} channel blocker LaCl_3 was added, the increase in cytosolic Ca^{2+} concentration and cellulase production induced by Mn^{2+} were effectively attenuated.

To investigate whether a cellulase increase, induced by Mn^{2+} , is associated with calcium signal transduction, we constructed a *crz1* deletion mutant Δcrz1 as Chen et al. [13] to block the calcium signal transduction pathway. As shown in Fig. 6a, b (Additional file 8: Figure S10A, B), the remarkable increase of CMCase and *pNPC*ase activities induced by Mn^{2+} , observed in parental strain Rut-C30, was effectively attenuated by deleting *crz1*. Similarly, the transcriptional levels of *cbh1* and *egl1* were markedly reduced in the Δcrz1 mutant at all time points examined (Fig. 6c, d).

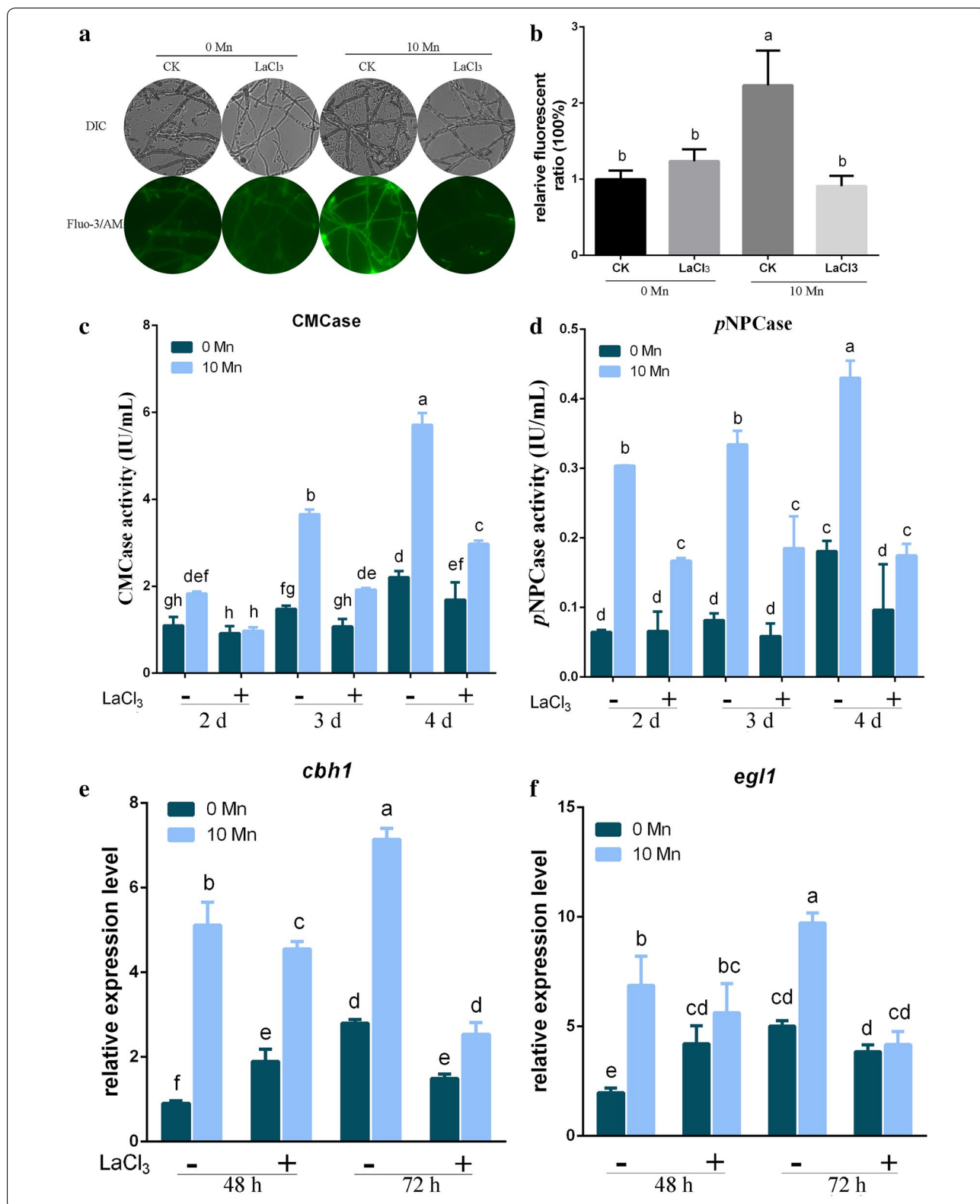
Taken together, these data indicated that Mn^{2+} induces cellulase improvement via calcium signal transduction in *T. reesei* Rut-C30. The improvement of cellulase production induced by Mn^{2+} is effectively prevented in a *crz1* mutant, blocking the calcium signal transduction pathway.

TPMR1 functions in conjunction with channels of *Mn*²⁺ and *Ca*²⁺

$\text{Mn}^{2+}/\text{Ca}^{2+}$ homeostasis exists in other fungi [33–36]. PMR1 plays an important role in $\text{Mn}^{2+}/\text{Ca}^{2+}$ homeostasis, and may act as a $\text{Ca}^{2+}/\text{Mn}^{2+}$ exchanger to balance Mn^{2+} via Ca^{2+} [17]. To clarify how Mn^{2+} increased cytosolic Ca^{2+} concentration, using *Neurospora crassa* PMR1 (GenBank: CAB65296.1) as the query, we searched for a PMR1 homolog (TRE119592) in the *T. reesei* genome, named as TPMR1.

(See figure on next page.)

Fig. 5 Effects of Ca^{2+} channel inhibitor LaCl_3 on the cytosolic Ca^{2+} concentration and cellulase production. **A** Fluorescence analysis of LaCl_3 influence on cytosolic Ca^{2+} burst induced by Mn^{2+} . The *T. reesei* Rut-C30 were cultured in liquid minimal medium for 48–60 h with 0 or 10 mM MnCl_2 (0 or 10 Mn, respectively), and then treated with 0 or 5 mM LaCl_3 . For detection, 50 μM Fluo-3/AM was used, and the intensity was monitored using Automatic Inverted Fluorescence Microscopy. Green fluorescence represents the free cytosolic Ca^{2+} . DIC, differential interference contrast, CK, not treated with LaCl_3 . **B** Comparative fluorescence ratio analysis of LaCl_3 influence on the cytosolic Ca^{2+} burst induced by Mn^{2+} . The y-axis represents the Ca^{2+} fluorescence ratio measured by CLSM and the x-axis the different treatments. The CMCase activity (**C**) and *pNPC*ase activity (**D**) of *T. reesei* Rut-C30 were examined after culture in medium containing 0 or 10 mM MnCl_2 and with (–) or without (+) 5 mM LaCl_3 . The expression levels of *cbh1* (**E**) and *egl1* (**F**) in *T. reesei* Rut-C30 were analyzed after culture in medium containing 0 or 10 mM MnCl_2 and with (–) or without (+) 5 mM LaCl_3 . Values are the mean \pm SD of the results from three independent experiments. Different letters indicate significant differences between the columns ($p < 0.05$, according to Duncan's multiple-range test)



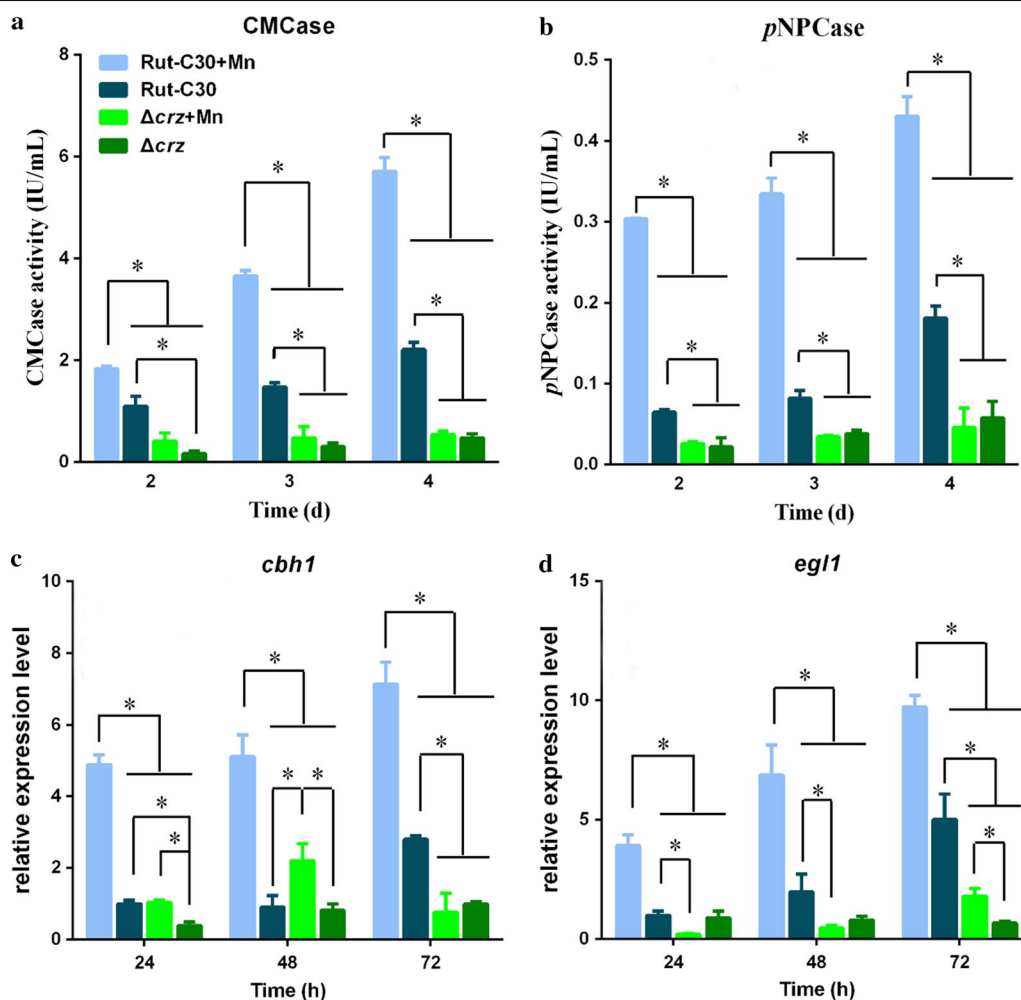


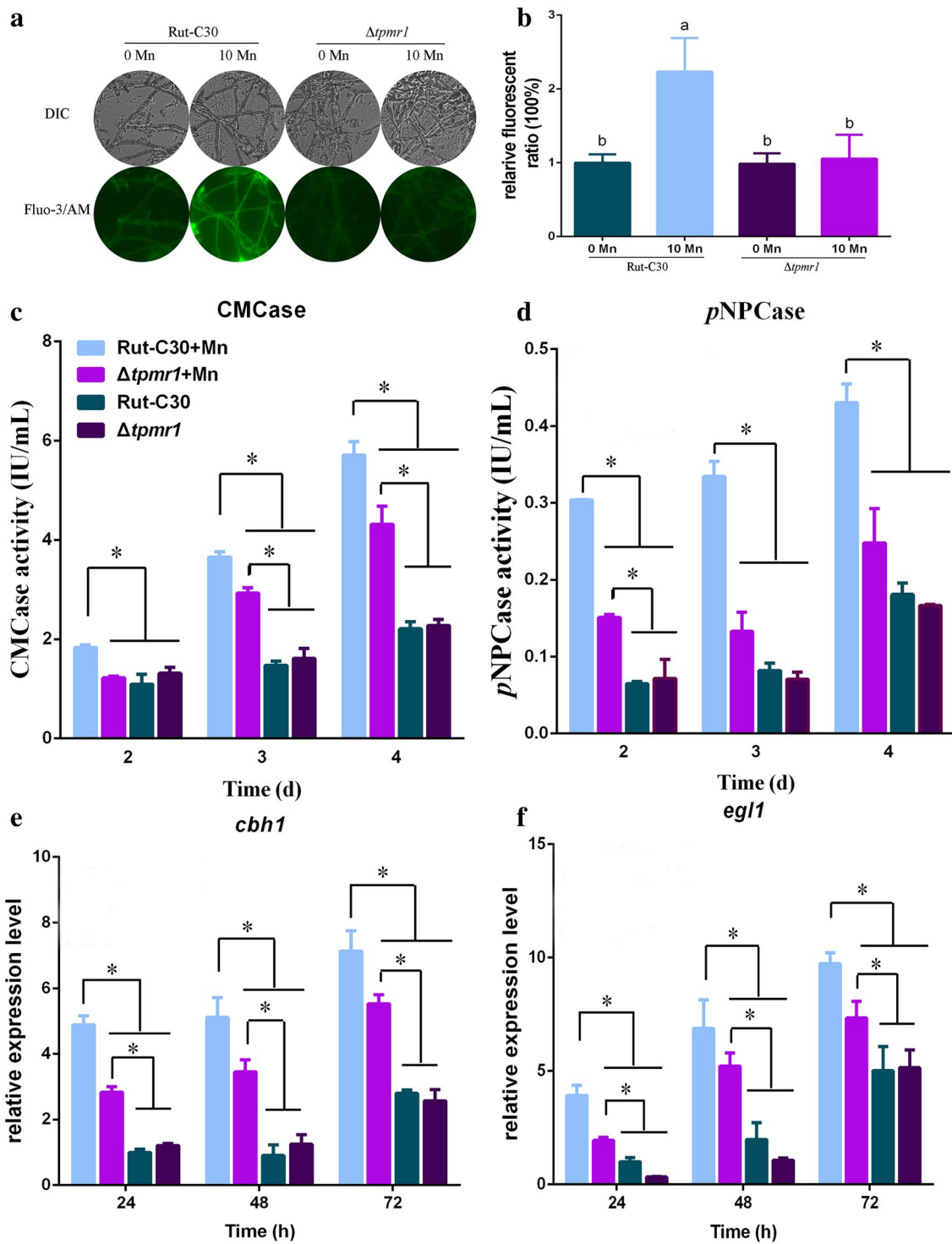
Fig. 6 Influence of CRZ1 on Mn^{2+} -induced cellulase production. The CMCase activity (**a**) and pNPCase activity (**b**) of *T. reesei* Rut-C30 and $\Delta crz1$ strains supplemented with 0 or 10 mM $MnCl_2$. The expression levels of *cbh1* (**c**) and *egl1* (**d**) in *T. reesei* Rut-C30 and $\Delta crz1$ strains supplemented with 0 or 10 mM $MnCl_2$. Values are the mean \pm SD of the results from three independent experiments. Asterisks indicate significant differences ($*p < 0.05$, Student's *t* test)

We constructed a *tpmr1* deletion mutant $\Delta tpmr1$. To investigate whether TPMR1 is responsible for pumping in Ca^{2+} upon 10 mM Mn^{2+} addition in *T. reesei*, we measured the level of intracellular Ca^{2+} in the $\Delta tpmr1$ strain

with or without Mn^{2+} addition. As shown in Fig. 7A and B, the increase in intracellular Ca^{2+} induced by Mn^{2+} in Rut-C30 was absent in the $\Delta tpmr1$ strain. The augmentation of Ca^{2+} levels induced by Mn^{2+} was blocked in

(See figure on next page.)

Fig. 7 Influence of TPMR1 on Mn^{2+} -induced cytosolic Ca^{2+} burst and cellulase production. **A** Fluorescence analysis of the influence of TPMR1 on the cytosolic Ca^{2+} burst induced by Mn^{2+} . The *T. reesei* Rut-C30 and $\Delta tpmr1$ strains were cultured in liquid minimal medium for 48–60 h with 0 or 10 mM $MnCl_2$ (0 or 10 Mn, respectively). For detection, 50 μM Fluo-3/AM was used, and the intensity was monitored using Automatic Inverted Fluorescence Microscopy. Green fluorescence represents the free cytosolic Ca^{2+} . DIC, differential interference contrast. **B** Comparative fluorescence ratio analysis of TPMR1 influence on cytosolic Ca^{2+} burst induced by Mn^{2+} . The y-axis represents the Ca^{2+} fluorescence ratio measured by CLSM and the x-axis the different treatments. The CMCase activity (**C**) and pNPCase activity (**D**) of *T. reesei* Rut-C30 and $\Delta tpmr1$ strains were examined after culture in medium containing 0 or 10 mM $MnCl_2$. The expression levels of *cbh1* (**E**) and *egl1* (**F**) in *T. reesei* Rut-C30 and $\Delta tpmr1$ strains were analyzed after culture in medium containing 0 or 10 mM $MnCl_2$. Values are the mean \pm SD of the results from three independent experiments. Asterisks indicate significant differences from untreated strains ($*p < 0.05$, $**p < 0.01$, Student's *t* test). Different letters indicate significant differences between the columns ($p < 0.05$, according to Duncan's multiple-range test)



the $\Delta tpmr1$ strain. These results suggested that TPMR1 is responsible for the increase of cytosolic Ca^{2+} under Mn^{2+} addition in *T. reesei* Rut-C30.

To further investigate the function of TPMR1 in conjunction with Mn^{2+} and Ca^{2+} channels, the intracellular and extracellular Mn^{2+} concentrations in the $\Delta tpmr1$ strain with or without Mn^{2+} addition were measured by ICP-MS during cultivation. As illustrated in Additional file 9: Figure S12, upon Mn^{2+} addition (10 mM final concentration), the intracellular Mn^{2+} concentration initially markedly increased, reaching and maintaining a high level after 24 h. The extracellular Mn^{2+} concentration dropped initially, reaching its minimum from 24 to 72 h. The intracellular and extracellular Mn^{2+} concentrations of the $\Delta tpmr1$ strain (Additional file 9: Figure S12) are quite different from that of Rut-C30 (Fig. 2a), whose intracellular Mn^{2+} gradually effused into the medium. These results suggested that TPMR1 is responsible for pumping Mn^{2+} out of the cell.

To further test the effect of TPMR1 on cellulase production under Mn^{2+} addition, we compared the cellulase production in parental strain Rut-C30 and $\Delta tpmr1$ mutant. Upon the addition of Mn^{2+} , the $\Delta tpmr1$ strain caused about 26 and 51% reductions in the CMCase and pNPCase activities, respectively, compared with that of Rut-C30 (Fig. 7C, D and Additional file 8: Figure S11A, B). Moreover, the transcriptional levels of *cbh1* and *egl1* observed are in agreement with the CMCase and pNPCase activity levels, which were markedly reduced in the $\Delta tpmr1$ mutant at all time points examined (Fig. 7E, F). The increase in cellulase production induced by Mn^{2+} was remarkably weakened in the *tpmr1* deletion mutant. These results demonstrated that TPMR1 functions in conjunction with channels of Mn^{2+} and Ca^{2+} in *T. reesei* Rut-C30.

Discussion

Metal ions are important in regulating cellular metabolism. For example, Ca^{2+} plays an important role in the regulation of cellulase or hemicellulase in *T. reesei* [13–15]. Paraszkiwicz et al. [37] reported Cd^{2+} , Zn^{2+} , and Pb^{2+} as environmental stress factors, which increased the biosynthesis of fungal emulsifier in *Curvularia lunata*. Addition of Ca^{2+} , Na^{+} , and Mn^{2+} enhanced ganoderic acid production in *Ganoderma lucidum* liquid cultures, through induction of the calcineurin signal pathway [17, 29, 38]. These results suggest that metal ions have significant impact on the cellular physiology and metabolism of various organisms. In this study, we first report that Mn^{2+} stimulates cellulase production and total protein secretion of *T. reesei* Rut-C30. However, whether other metal ions or stimuli have an impact on cellulase production of *T. reesei* will require further evidence for confirmation.

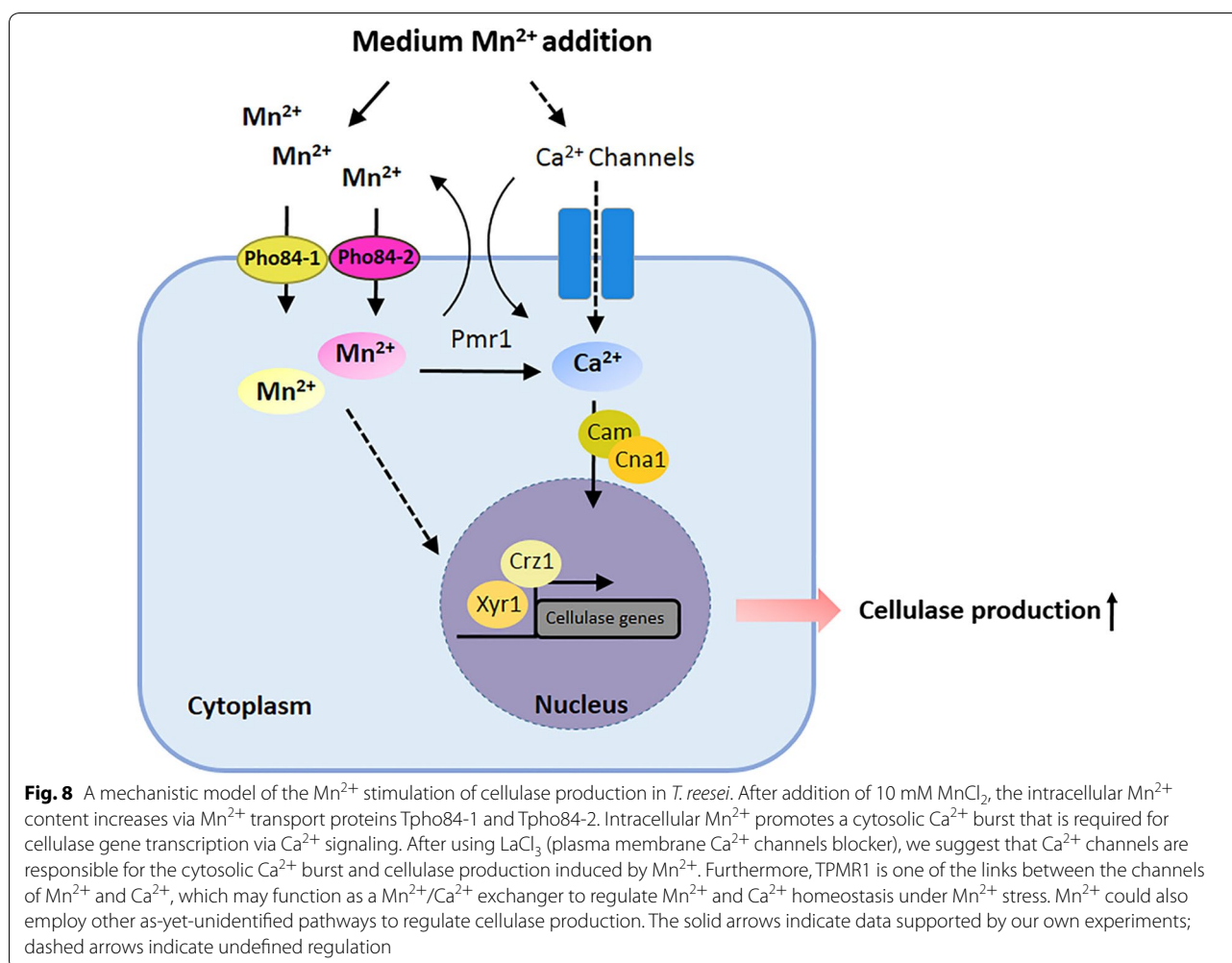
Diverse Mn^{2+} transports have been identified in the yeasts, plants, and bacteria [21, 22, 39–42]. Mn^{2+} can enter the cell through two different routes including high- and low-affinity transporters [21, 22, 41, 42]. SMF1, a plasma membrane NRAM (Natural Resistance-Associated Macrophage Protein) family Mn^{2+} transporter, is a high-affinity transporter for Mn^{2+} , contributing to Mn^{2+} accumulation under extreme Mn^{2+} starvation conditions [16, 22, 43, 44]. PHO84, a family of phosphate/proton symporters [45], can transport Mn^{2+} under excess Mn^{2+} stress [16, 25], indicating that PHO84 is a low-affinity transporter of Mn^{2+} , contributing to Mn^{2+} accumulation only when cells are exposed to higher Mn^{2+} concentrations. *T. reesei* might contain both high- and low-affinity transporters of Mn^{2+} , similar to what has been described for the metal transport systems for iron, copper, and zinc [46–50]. A BLAST search of the genome sequence of *T. reesei* identified a gene (*tre79644*) similar to SMF1, and this gene was named *tsmf1*. There was no significant difference on Mn^{2+} transport and cellulase production under 10 mM Mn^{2+} surplus using a *tsmf1* deletion strain (data not shown). The alternative PHO84 homologs remain to be identified in *T. reesei* Rut-C30. Five candidates including TPHO84-1 and TPHO84-2 are similar to PHO84. We proved that extracellular Mn^{2+} is transported into Rut-C30 cells via TPHO84-1 and TPHO84-2, which are annotated as putative low-affinity transports of Mn^{2+} responding to higher Mn^{2+} concentration. Meanwhile, there were no significant differences between the cytosolic Ca^{2+} concentrations for the *T. reesei* Rut-C30, $\Delta tpho84-1$, $\Delta tpho84-2$, and $\Delta tpho84-1/2$ mutants (see Additional file 10: Figure S13).

Calcium is widely used as a second messenger in prokaryotic and eukaryotic cells. It is known that a cytosolic Ca^{2+} burst and further induced calcium signaling regulate cellular responses when exposed to different external stimuli [51, 52]. For instance, Na^{+} induction enhances cytosolic Ca^{2+} to induce the ganoderic acid biosynthesis through calcineurin signal pathway, to upregulate its biosynthetic genes at the transcriptional level in *Ganoderma lucidum* [29]. High temperatures are known to trigger the generation of cytosolic Ca^{2+} in plants [53]. Alkaline pH triggers an immediate calcium burst in *Candida albicans* [54]. Our results indicated that Mn^{2+} induces a significantly increased cytosolic Ca^{2+} level in *T. reesei* Rut-C30 (Fig. 4A, B). Additionally, in our experiments, inhibition of cytosolic Ca^{2+} level by LaCl_3 effectively attenuated the cellulase increase induced by Mn^{2+} (Fig. 5C–E). The results showed that 10 mM Mn^{2+} stress led to a cytosolic Ca^{2+} burst in *T. reesei* Rut-C30. An earlier study demonstrated that Ca^{2+} (/calmodulin)–calcineurin–CRZ1 signaling could induce cellulase production at the transcription level by Ca^{2+}

stimulation [13]. In our study, Mn^{2+} could also activate the expression of Ca^{2+} (calmodulin)–calcineurin–CRZ1 signaling-related genes in *T. reesei* Rut-C30 (Fig. 4C–E). Furthermore, CRZ1 participated in regulating cellulase production in Mn^{2+} -induced strains (Fig. 6a–d). The results presented here indicate that the regulation of cellulase gene expression and production by Mn^{2+} are dependent on cytosolic Ca^{2+} burst and further induce calcium signaling.

PMR1, encoding the Ca^{2+}/Mn^{2+} P-type ATPase, is required to either scavenge trace amounts of Mn^{2+} and Ca^{2+} from the medium or maintain sufficient levels of Mn^{2+} and Ca^{2+} in an intracellular compartment [22, 24–26, 33]. Bowman et al. [33] reported that a *pmr1* deletion strain accumulates 80% lesser Ca^{2+} than the wild type. Under higher levels of intracellular Mn^{2+} , extracellular Ca^{2+} might transport into the cells through PMR1 to increase intracellular Ca^{2+} and then trigger calcium signaling to regulate cellular responses [35]. Our work found that the increase in Ca^{2+} levels induced by Mn^{2+}

treatment was blocked in the *tpmr1* deletion strain (Fig. 7A, B) and that the improvement of cellulase production induced by Mn^{2+} was remarkably weakened in the *tpmr1* deletion mutant. These results demonstrated that TPMR1 functions as a channel of Mn^{2+} and Ca^{2+} in *T. reesei* Rut-C30. Cytosolic Ca^{2+} concentration was enhanced through TPMR1 under Mn^{2+} addition, thus inducing calcium signaling to upregulate cellulase genes. Additionally, PMR1 provides a major route for cellular sequestration of Mn^{2+} by pumping excess Mn^{2+} into the Golgi, from where the metal may exit the cell via the secretory pathway vesicles that merge with the cell surface and release the Mn^{2+} contents back into the extracellular environment [20, 22, 24, 34]. These data correlate well with our data indicating that intracellular Mn^{2+} gradually effused to the medium from 24 h (Fig. 2a). However, in the Δ *tpmr1* mutant, the intracellular Mn^{2+} concentration maintained its high level after 24 h, and the extracellular Mn^{2+} concentration reached its minimum from 24 to 72 h. These results implied that TPMR1



participates in pumping excess Mn^{2+} into the Golgi, and then releases it extracellularly, meanwhile accumulating cytosolic Ca^{2+} in *T. reesei* Rut-C30. However, the detailed role of TPMP1 in *T. reesei* needs further research.

We found that 10 mM Mn^{2+} could also stimulate cellulase production and increase total protein secretion from the *T. reesei* wild-type strain QM6a and the mutant strain Qm9414 (data not shown). However, the results from Rut-C30 may not be identical to those of the wild-type strain, because each strain likely has its own unique regulatory mechanism.

Conclusions

In summary, the putative mechanism of the extracellular Mn^{2+} -induced stimulation of cellulase production was characterized in *T. reesei* Rut-C30 (Fig. 8). Mn^{2+} induces a significantly increased cytosolic Ca^{2+} level and triggers Ca^{2+} -CRZ1 signaling to induce cellulase production at the transcription level. Moreover, we identified two Mn^{2+} transport proteins in *T. reesei* Rut-C30, and named TPHO84-1 and TPHO84-2. Furthermore, TPMP1 acts as a link between channels in Mn^{2+} and Ca^{2+} homeostasis in *T. reesei*. This study provides a successful approach to produce a higher yield of cellulase and to develop industrially applicable *T. reesei* strains, which is important for biofuel production from lignocellulose. This study also provides a molecular basis for understanding the regulatory mechanism of divalent metal ions on the cellular metabolism of fungi.

Methods

Strains and growth conditions

Escherichia coli DH5 α was used for plasmid amplification. *Agrobacterium tumefaciens* strain AGL-1 was used as a T-DNA donor for fungal transformation [55]. *T. reesei* Rut-C30 (ATCC 56765) was used throughout the study and as the host for genetic transformation. Luria–Broth (LB) was used for culture of *E. coli* and *A. tumefaciens*. Mandels' medium [56] was used for the general fungal culture. All strains were maintained on potato dextrose agar (PDA) plates at 28 °C. The fungal strains constructed in this study are summarized in Table 1. All strains were cultured in the dark.

Minimal medium (MM, $(NH_4)_2SO_4$ 5 g/l; Urea 0.3 g/l; KH_2PO_4 15 g/l; $CaCl_2$ 0.6 g/l; $MgSO_4$ 0.6 g/l; $FeSO_4 \cdot 7H_2O$ 5 mg/l; $ZnSO_4 \cdot 7H_2O$ 1.4 mg/l; $CoCl_2 \cdot 6H_2O$ 2 mg/l; pH 5.5) with 2% glucose was used to assess the effect of Mn^{2+} on hyphal growth. To analyze the effects of Mn^{2+} on cellulase activity, protein concentration, and gene expression levels, medium replacement experiments were performed. After growth in Mandels' medium with 2% glucose for ~ 32 h at 28 °C and 220 rpm, approximately 0.1 g of mycelia were collected and washed thoroughly

Table 1 *T. reesei* strains constructed in this study

Strains	Relevant features	Source
Rut-C30	Parent strain	ATCC
$\Delta tpo84-1(\Delta 77552)$	Rut-C30-deleted <i>tpo84-1</i> gene	This study
$\Delta tpo84-2(\Delta 45868)$	Rut-C30-deleted <i>tpo84-2</i> gene	This study
$\Delta tpo84-1/2$	Rut-C30-deleted <i>tpo84-1</i> and <i>tpo84-2</i> gene	This study
$\Delta 81389$	Rut-C30-deleted <i>tre81389</i> gene	This study
$\Delta 45852$	Rut-C30-deleted <i>tre45852</i> gene	This study
$\Delta 106118$	Rut-C30-deleted <i>tre106118</i> gene	This study
<i>rfp-tpo84-1</i>	Rut-C30-harboring vector <i>prfp-tpo84-1</i>	This study
<i>rfp-tpo84-2</i>	Rut-C30-harboring vector <i>prfp-tpo84-2</i>	This study
<i>tpo84-1-rc</i>	Rut-C30-harboring vector <i>ptpo84-1-rc</i>	This study
<i>tpo84-2-rc</i>	Rut-C30-harboring vector <i>ptpo84-2-rc</i>	This study
$\Delta crz1$	Rut-C30-deleted <i>crz1</i> gene	This study
$\Delta tpmr1$	Rut-C30-deleted <i>tpmr1</i> gene	This study

using 0.85% NaCl, then transferred to 100 ml MM containing 1% (w/v) Avicel (PH-101, Sigma-Aldrich) with the addition of $MnCl_2$ to final concentrations of 1, 10, 20, and 40 mM. Strains were induced for 1–5 days before being subjected to testing for enzymatic activity, protein concentration, or induced for 24, 48, or 72 h before being subjected to RNA extraction and RT-qPCR analyses, respectively. To assess the effect of plasma membrane Ca^{2+} channels on the regulation of cellulase production of *T. reesei* Rut-C30, 5 mM (final concentration) $LaCl_3$ (Aladdin, Shanghai, China) was added after 1 day of culture in MM.

Fungal growth, enzymatic activity, protein concentration, and biomass assays

For fungal hyphal growth assays, conidia were collected and diluted to 10^7 ml⁻¹ in sterile water. An equal volume of the solution (2 μ l) was inoculated onto the center of the MM plates as described above, and was grown for 3–5 days at 28 °C.

For enzymatic activity, protein concentration, and biomass assays, 1 ml of culture liquid was collected and subjected to 0.45- μ m filtration. The culture supernatants were subjected to cellulase activity and protein concentration analysis. The mycelia were subjected to biomass measurement. Fungal CMCase and *p*NPCase activities were measured according to the method described by Wang et al. [57]. Protein concentrations were determined using the Bradford Protein Assay Kit (Generay, Shanghai, China). Biomass concentration was indirectly measured by calculating the amount of total intracellular proteins, with some modification [58]. Briefly, harvested mycelia

were suspended in 1 ml 1 M NaOH in a reaction tube and the mixture was incubated for 2 h and frequently vortexed. Total protein was collected via centrifugation at $14,000\times g$ at 4 °C for 10 min. Total protein concentration was determined by the Modified Lowry Protein Assay Kit (Sangon Biotech, Shanghai, China). The final protein content was furthermore corrected using a set of substrate controls where no inoculum was added to the medium. The biomass dry weight was then calculated assuming an average content of 0.32 g intracellular protein per gram of dry cell mass.

RNA isolation and quantitative real-time reverse-transcription polymerase chain reaction (RT-qPCR)

The levels of gene-specific mRNA were assessed using RT-qPCR, according to our previous study, with some modification [59]. In brief, the total RNA of 50 mg fresh weight cells was extracted using a FastRNA Pro Red Kit (MPbio, Irvine, CA, USA), according to the manufacturer's instructions. Synthesis of cDNA from total RNA was performed using the PrimeScript RT Reagent Kit with gDNA eraser (TaKaRa, Japan) as per the manufacturer's instructions. For RT-qPCR, the TransStart TipTop Green qPCR SuperMix (TransGen, Shanghai, China) was used with 200 nM of forward and reverse primers (see Additional file 1: Table S1). Gene transcription was analyzed using SYBR green assays. Transcription levels of target genes were normalized to that of the *sar1* gene [60]. Thermocycling was performed in an ABI StepOne Plus thermocycler (Applied Biosystems, Foster City, CA, USA).

Determination of extracellular and intracellular Mn²⁺ concentration

Extracellular and intracellular Mn²⁺ concentrations were measured by inductively coupled plasma mass spectrometry (ICP-MS), as described for *Ganoderma lucidum* by Xu [17]. Five milliliter of culture liquid was collected and subjected to filtration. The culture supernatant and mycelium were subjected to extracellular and intracellular Mn²⁺ concentrations, respectively. The supernatant of the cultures was filtered through 0.22- μ m membranes and then diluted with 1% HNO₃ for measuring the extracellular Mn²⁺ concentration. Mycelia were washed in distilled water to remove any nonspecifically bound Mn²⁺, and digested with 1 ml 68% HNO₃. The mixture was collected via centrifugation at $12,000\times g$ for 5 min. The supernatant was then filtered through a 0.22- μ m membrane and diluted with 1% HNO₃ for measuring intracellular Mn²⁺ concentration. The final intracellular Mn²⁺ concentration was shown as micromole per gram biomass.

Construction of plasmids and strains

To construct a *tpho84-1* deletion mutant, the upstream (− 1 to − 762 bp) and downstream (+ 1917 to + 2681 bp) fragments of *tpho84-1* were generated from the genome of *T. reesei* Rut-C30 using KOD-Plus-Neo (TOYOBO, Japan). All primers are indicated in Additional file 1: Table S1. First, the upstream fragment was ligated into the *PacI*- and *XbaI*-linearized LML2.0 [61] using the ClonExpress™ II One Step Cloning Kit (Vazyme, Nanjing, China) to form pF*tpho84-1*. Subsequently, the downstream fragment was inserted into *SwaI*-linearized pF*tpho84-1* to form the binary vector pD*tpho84-1* (see Additional file 5: Figure S4A) for the knockout of *tpho84-1* in Rut-C30 using *Agrobacterium*-mediated transformation [59]. Strains were selected using hygromycin B and cefotaxime on Mandels' medium. Then, the marker was excised using the method described by Zhang [61]. The putative *tpho84-1* disruption mutants (Δ *tpho84-1*/ Δ 77552) generated by double crossover were verified by diagnostic PCR using the primers *tpho84-1*-CF and *tpho84-1*-CR and *tpho84-1*-OF and *tpho84-1*-OR (see Additional file 5: Figure S4E).

Similarly, the 706-bp upstream and 710-bp downstream regions of *tpho84-2* were amplified and then inserted into LML2.0 as described above to generate the binary vector pD*tpho84-2* (see Additional file 5: Figure S4B). After transformation and selection, the putative *tpho84-2* deletion mutant (Δ *tpho84-2*/ Δ 45868) was verified by diagnostic PCR using the primers *tpho84-2*-CF and *tpho84-2*-CR, and *tpho84-2*-OF and *tpho84-2*-OR (see Additional file 5: Figure S4E). The *tre81389*, *tre45852*, *tre106118*, *crz1*, and *tpmr1* disruption mutants (Δ 81389, Δ 45852, Δ 106118, Δ *crz1*, and Δ *tpmr1*) were constructed similarly (see Additional file 11: Figure S14).

To construct a *tpho84-1/2* deletion mutant, the pD*tpho84-2* cassette was transformed into Δ *tpho84-1* strain using *Agrobacterium*-mediated transformation. The *tpho84-1/2* double deletion mutant (Δ *tpho84-1/2*) was verified by diagnostic PCR.

For *tpho84-1* and *tpho84-2* re-complementation, 3916- and 4087-bp DNA fragments containing total *tpho84-1* and *tpho84-2* expression cassette were amplified from the Rut-C30 genome using *tpho84-1*-rc-1/*tpho84-1*-rc-2 and *tpho84-2*-rc-1/*tpho84-2*-rc-2, and then inserted into *SwaI*-linearized LML2.0 to generate vector *ptpho84-1*-rc and *ptpho84-2*-rc, respectively. *Ptpho84-1*-rc and *ptpho84-2*-rc were then transferred to the *tpho84-1* and *tpho84-2* deletion strain by *Agrobacterium*-mediated transformation (see Additional file 5: Figure S4C, D). *tpho84-1* and *tpho84-2* re-complementation strains (*tpho84-1*-rc and *tpho84-2*-rc) were selected and verified by PCR using *tpho84-1*-OF and *tpho84-1*-OR, and

tpho84-2-OF and tpho84-2-OR (see Additional file 5: Figure S4F).

For the construction of N-terminal RFP-tagged translational fusion of *tpho84-1* under the control of the *cbh1* promoter, the upstream (− 1 to − 1038 bp) and downstream (+ 1 to + 1084 bp) fragments of *tpho84-1* were generated from the genome of *T. reesei* Rut-C30 using KOD-Plus-Neo (TOYOBO, Japan). The promoter of *cbh1* (P_{cbh1}) was obtained by PCR from the genome of *T. reesei* Rut-C30. Red fluorescent protein (*rfp*) was obtained by PCR using the plasmid pDsRed2-N1 (Clontech) as the template. First, the upstream fragment was ligated into the *PacI*- and *XbaI*-linearized LML2.0, using the ClonExpress™ II One Step Cloning Kit (Vazyme, Nanjing, China) to form pFr*tpho84-1*. Subsequently, the P_{cbh1} , *rfp*, and downstream fragments were inserted into *SwaI*-linearized Fr*tpho84-1* to form the binary vector pRFP-TPHO84-1 for subcellular location of *tpho84-1* using *Agrobacterium*-mediated transformation. Subsequently, the marker was excised following the method of Zhang [61]. The putative *rfp-tpho84-1* mutants (*rfp-tpho84-1*) generated by double crossover were verified by diagnostic PCR using the primers *rfp-tpho84-1*-CF and *rfp-tpho84-1*-CR (see Additional file 12: Figure S15).

Similarly, the 997-bp upstream and 797-bp downstream regions of *tpho84-2* were amplified and then inserted into LML2.0 as described above to generate the binary vector pRFP-TPHO84-2 (see Additional file 6: Figure S5A). After transformation and selection, the putative *rfp-tpho84-2* mutants (*rfp-tpho84-2*) was verified by diagnostic PCR using the primers *rfp-tpho84-2*-CF and *rfp-tpho84-2*-CR (see Additional file 12: Figure S15).

The genome sequence of *T. reesei* is available at the US Department of Energy (DOE) Joint Genome Institute (<http://genome.jgi-psf.org/Trire2/Trire2.home.html>).

Fluorescence microscopy

To localize RFP-TPHO84-1/2 fusion proteins using microscopy, the *rfp-tpho84-1* and *rfp-tpho84-2* strains were inoculated into Mandels' medium and grown for 48–60 h. The mycelia were then observed using an S Plan Fluor ELWD 100×, 1.3 numerical aperture (NA) objective on a Laser Scanning Confocal Microscope (A1R, Nikon, Japan) comprising a Texas Red filter (500–620 nm band-pass excitation filter and emission filter of 670 nm). Images were processed using the NIS elements software (Nikon).

Free cytosolic Ca²⁺ labeling and detection

Fluo-3/AM (Sigma) was used as a Ca²⁺-specific probe to assess the level of cytoplasmic Ca²⁺ in *T. reesei* Rut-C30 according to the manufacturer's protocol. Fluo-3/AM (50 μM final concentration) was loaded into cells by

incubation at 37 °C for 30 min, and the cells were then washed three times with phosphate-buffered saline. Images of Ca²⁺ green fluorescence were observed using an S Plan Fluor ELWD 20×, 0.5 numerical aperture (NA) objective and a digital sight camera on an Eclipse Ti inverted microscope system (Ti-E, Nikon, Japan), comprising an FITC filter (420–490 nm band-pass excitation filter, and emission filter of 535 nm). The intensity of green fluorescence was quantified using NIS-Elements F package software. To eliminate the contribution of background fluorescence, cells without Fluo-3/AM labeling were also imaged under identical conditions.

Statistical analysis

All experimental data shown in this paper were carried out at least three times with identical or similar results. For every experiment, three biological replicates were performed with three technical replicates. The error bars indicate the standard deviation (SD) from the mean of triplicates. Student's *t* test was used to compare two samples. Duncan's multiple-range test was used for multiple comparisons. *p* < 0.05 was considered to be significant.

Additional files

Additional file 1: Table S1. Primers used in this study.

Additional file 2: Figure S1. Influence of Mn²⁺ on the transcriptional levels of cellulase-encoding genes in *T. reesei* Rut-C30. **A–E** The effects of Mn²⁺ on the transcriptional levels of *cbh1* (A), *cbh2* (B), *xyr1* (C), *egl1* (D) and *egl2* (E). 0 Mn, no Mn²⁺ was added to the medium; 10 Mn, final concentration of 10 mM. Three independent experiments with three biological replicates each were performed. Values are the means ± SD of the results from three independent experiments. Asterisks indicate significant differences from untreated strains (**p* < 0.05, ***p* < 0.01, Student's *t* test).

Additional file 3: Figure S2. Influence of Mn²⁺ addition on the transcriptional levels of putative Mn²⁺ transport-encoding genes. **A–E** The effect of Mn²⁺ on the transcriptional levels of *tre77552* (A), *tre81389* (B), *tre45852* (C), *tre45868* (D), and *tre106118* (E). 0 Mn, no Mn²⁺ was added to the medium; 10 Mn, final concentration of 10 mM. Values are the means ± SD of the results from three independent experiments. Asterisks indicate significant differences from untreated strains (**p* < 0.05, Student's *t* test).

Additional file 4: Figure S3. Concentrations of Mn²⁺ in *T. reesei* Rut-C30 and its derivative mutants. The concentrations of intracellular Mn²⁺ of *T. reesei* Rut-C30 and its derivative mutant strains were examined after cultured in medium containing 10 mM MnCl₂. Values are the means ± SD of the results from three independent experiments. Asterisks indicate significant differences from parental strain Rut-C30 (**p* < 0.05, Student's *t* test).

Additional file 5: Figure S4. Construction and verification of Δ *tpho84-1*, Δ *tpho84-2*, *tpho84-1-rc*, *tpho84-2-rc* mutants. (A) Schematic representation of the *tpho84-1* locus from Rut-C30 and Δ *tpho84-1* mutant. The binding sites of primers on the genome of Rut-C30 and Δ *tpho84-1*, and the expected sizes of the products in PCR verification are given. The region from +1 to +1916 bp relative to the translation start site of *tpho84-1* (grey box) was replaced with the hygromycin resistance expression cassette (hygromycin, black box). (B) Schematic representation of the *tpho84-2* locus from Rut-C30 and Δ *tpho84-2* mutant. The binding sites of primers

on the genome of Rut-C30 and $\Delta tpo84-2$ and the expected sizes of the PCR products are given. The region from +1 to +2087 bp relative to the translation start site of *tpo84-2* (grey box) was replaced with the hygromycin resistance expression cassette (hygromycin, black box). (C) Schematic representation of the P-*tpo84-1*-*tpo84-1*-T-*tpo84-1* cassette in *tpo84-1-rc* strains. The primer pairs indicated were used in the verification of the expression cassette. P-*tpo84-1*, the possible promoter of *tpo84-1*; T-*tpo84-1*, the possible terminator of *tpo84-1*. (D) Schematic representation of the P-*tpo84-2*-*tpo84-2*-T-*tpo84-2* cassette in *tpo84-2-rc* strains. The primer pairs indicated were used in the verification of the expression cassette. P-*tpo84-2*, the possible promoter of *tpo84-2*; T-*tpo84-2*, the possible terminator of *tpo84-2*. (E) PCR verification of the $\Delta tpo84-1$ and $\Delta tpo84-2$ mutants. Lane M, DNA molecular mass maker. PCR amplification results of the D*tpo84-1*-F were obtained using *tpo84-1*-CF with D70-4 and D*tpo84-1*-R were obtained using HG3.6 with *tpo84-1*-CR (see Additional file 1: Table S1). PCR amplification results of the D*tpo84-2*-F were obtained using *tpo84-2*-CF with D70-4 and D*tpo84-2*-R were obtained using HG3.6 with *tpo84-2*-CR. (F) PCR verification of the *tpo84-1-rc* and *tpo84-2-rc* strains. Lane M, DNA molecular mass maker. PCR amplification results of the *tpo84-1-rc* were obtained using *tpo84-1*-OF with *tpo84-1*-OR and *tpo84-2-rc* was obtained using *tpo84-2*-OF with *tpo84-2*-OR. The genome of the $\Delta tpo84-1$ and $\Delta tpo84-2$ mutants were used as a negative control.

Additional file 6: Figure S5. Subcellular localization of TPHO84-1 and TPHO84-2. Schematic representation of the plasmids used for expression of RFP-TPHO84-1 and RFP-TPHO84-2. RFP was fused to the N-terminal of TPHO84-1 and TPHO84-2 and expressed under the control of the *cbh1* promoter. **B.** In vivo epifluorescence analysis of *rfp-tpo84-1* and *rfp-tpo84-2* transformants. The transformants were cultured in liquid Mandel's medium for 48–60 h and observed using Laser Scanning Confocal Microscopy.

Additional file 7: Figure S6. Cellulase activities of *T. reesei* Rut-C30 and its derivative mutant strains. The activities were examined after cultured in medium containing 0 mM Mn²⁺. (A) CMCase activities, (B) pNPCase activities. Values are the means \pm SD of the results from three independent experiments.

Additional file 8. Data for corresponding cellulase activity per biomass. The CMCase/biomass activity and pNPCase/biomass activity of *T. reesei* strains were examined. For every experiment, three biological replicates were performed with three technical replicates each. Values are the means \pm SD of the results from three independent experiments. Asterisks indicate significant differences ($*p < 0.05$, Student's *t* test).

Additional file 9: Figure S12. Concentrations of Mn²⁺ in $\Delta tpmr1$ strain. The concentrations of extracellular and intracellular Mn²⁺ of the $\Delta tpmr1$ strain was examined after culturing in minimal medium containing 0 or 10 mM MnCl₂. Filled circle, intracellular Mn²⁺ concentration after adding 10 mM MnCl₂; blank circle, extracellular Mn²⁺ concentration after adding 10 mM MnCl₂; filled square, intracellular Mn²⁺ concentration of control without MnCl₂ supplementation; blank square, extracellular Mn²⁺ concentration of control without MnCl₂ supplementation. Values are the means \pm SD of the results from three independent experiments.

Additional file 10: Figure S13. Cytosolic Ca²⁺ levels increase after Ca²⁺ addition. **A.** The analysis of cytosolic Ca²⁺ levels via a Ca²⁺ fluorescent probe Fluo-3/AM. The *T. reesei* Rut-C30 and its derivative mutant strains were cultured in liquid minimal medium (initial 5.4 mM Ca²⁺) for 48–60 h with extra 0 or 10 mM CaCl₂ supplementation (low Ca or high Ca, respectively). For detection, 50 μ M Fluo-3/AM was used, and the intensity was monitored using Automatic Inverted Fluorescence Microscopy. Green fluorescence represents the free cytosolic Ca²⁺. DIC, differential interference contrast. **B.** Comparative fluorescence ratio analysis of Ca²⁺ influence on cytosolic Ca²⁺ levels. The y-axis represents the Ca²⁺ fluorescence ratio measured by CLSM, and the x-axis represents the different strains tested.

Additional file 11: Figure S14. Verification of $\Delta 81389$, $\Delta 45852$, $\Delta 106118$, $\Delta crz1$, and $\Delta tpmr1$ mutants. Lane M, DNA molecular mass maker. PCR amplification results of the F were obtained using t81389-, t45852-,

t106118-, tcrz1-, and tpmr1-CF, respectively, with D70-4, and R were obtained using HG3.6 with t81389-, t45852-, t106118-, tcrz1-, and tpmr1-CR, respectively. PCR amplification using primer pairs t81389-, t45852-, t106118-, tcrz1-, and tpmr1-OF/OR, respectively, was performed as a negative confirm for gene deletion.

Additional file 12: Figure S15. PCR Verification of *rfp-tpo84-1*, *rfp-tpo84-2* mutants. Lane M, DNA molecular mass marker. PCR amplification results of the *rfp-tpo84-1*-F were obtained using *rfp-tpo84-1*-CF with D70-4 and *rfp-tpo84-1*-R were obtained using HG3.6 with *rfp-tpo84-1*-CR (Additional file 1: Table S1). PCR amplification results of the *rfp-tpo84-2*-F were obtained using *rfp-tpo84-2*-CF with D70-4 and *rfp-tpo84-2*-R were obtained using HG3.6 with *rfp-tpo84-2*-CR.

Abbreviations

crz1: calcineurin-responsive zinc finger transcription factor 1; CMCase: endo- β -glucanase activity; pNPCase: exo- β -glucanase activity; qRT-PCR: quantitative reverse-transcription PCR; ICP-MS: inductively coupled plasma mass spectrometry; NRAMP: Natural Resistance-Associated Macrophage Protein.

Authors' contributions

WW initiated, designed, and coordinated the study and reviewed the manuscript. YC planned and carried out experiments and measurements, and interpreted experimental data. DW and WW supported the research funding. All authors read and approved the final manuscript.

Acknowledgements

Not applicable.

Competing interests

The authors declare that they have no competing interests.

Availability of data and materials

All data generated or analyzed during this study are included in this published article [and in Additional files 1 and 2].

Consent for publication

Not applicable.

Ethics approval and consent to participate

Not applicable.

Funding

This research was supported by the National Natural Science Foundation of China [No. C010302-3150066], and the Fundamental Research Funds for the Central Universities [No. 222201714053].

Publisher's Note

Springer Nature remains neutral with regard to jurisdictional claims in published maps and institutional affiliations.

Received: 16 November 2017 Accepted: 18 February 2018

Published online: 01 March 2018

References

- Cherry JR, Fidantsef AL. Directed evolution of industrial enzymes: an update. *Curr Opin Biotechnol*. 2003;14:438–43.
- Jun H, Kieselbach T, Jönsson LJ. Enzyme production by filamentous fungi: analysis of the secretome of *Trichoderma reesei* grown on unconventional carbon source. *Microb Cell Fact*. 2011;10:68.
- Kubicek CP, Mikus M, Schuster A, Schmöll M, Seiboth B. Metabolic engineering strategies for the improvement of cellulase production by *Hypocrea jecorina*. *Biotechnol Biofuels*. 2009;2:19.

4. Schuster A, Schmoll M. Biology and biotechnology of *Trichoderma*. Appl Microbiol Biotechnol. 2010;87:787–99.
5. Bischof RH, Ramoni J, Seiboth B. Cellulases and beyond: the first 70 years of the enzyme producer *Trichoderma reesei*. Microb Cell Fact. 2016;15:106.
6. Ramoni J, Marchetti-Deschmann M, Seidl-Seiboth V, Seiboth B. *Trichoderma reesei* xylanase 5 is defective in the reference strain QM6a but functional alleles are present in other wild-type strains. Appl Microbiol Biotechnol. 2017;101:4139–49.
7. Dashtban M, Buchkowski R, Qin W. Effect of different carbon sources on cellulase production by *Hypocrea jecorina* (*Trichoderma reesei*) strains. Int J Biochem Mol Biol. 2011;2:274–86.
8. Jourdir E, Cohen C, Poughon L, Larroche C, Monot F, Ben Chaabane F. Cellulase activity mapping of *Trichoderma reesei* cultivated in sugar mixtures under fed-batch conditions. Biotechnol Biofuels. 2013;6:79.
9. Stricker AR, Mach RL, de Graaff LH. Regulation of transcription of cellulases- and hemicellulases-encoding genes in *Aspergillus niger* and *Hypocrea jecorina* (*Trichoderma reesei*). Appl Microbiol Biotechnol. 2008;78:211–20.
10. Seibel C, Gremel G, Silva RD, Schuster A, Kubicek CP, Schmoll M. Light-dependent roles of the G-protein α subunit GNA1 of *Hypocrea jecorina* (anamorph *Trichoderma reesei*). BMC Biol. 2009;7:58.
11. Tisch D, Kubicek CP, Schmoll M. New insights into the mechanism of light modulated signaling by heterotrimeric G-proteins: ENVOY acts on *gna1* and *gna3* and adjusts cAMP levels in *Trichoderma reesei* (*Hypocrea jecorina*). Fungal Genet Bio. 2011;48:631–40.
12. Stranks DW. Influence of phenethyl alcohol and other organic solvents on cellulase production. Can J Microbiol. 1973;19:1523–6.
13. Chen L, Zou G, Wang J, Wang J, Liu R, Jiang Y, Zhao G, Zhou Z. Characterization of the Ca^{2+} -responsive signaling pathway in regulating the expression and secretion of cellulases in *Trichoderma reesei* Rut-C30. Mol Microbiol. 2016;100:560–75.
14. Mach RL, Zeilinger S, Kristufek D, Kubicek CP. Ca^{2+} -calmodulin antagonists interfere with xylanase formation and secretion in *Trichoderma reesei*. Biochim Biophys Acta. 1998;1403:281–9.
15. Mandels M, Reese ET. Induction of cellulase in *Trichoderma viride* as influenced by carbon sources and metals. J Bacteriol. 1957;73:269–78.
16. Jensen LT, Ajaia-Alemanji M, Culotta VC. The *Saccharomyces cerevisiae* high affinity phosphate transporter encoded by *PHO84* also functions in manganese homeostasis. J Biol Chem. 2003;278:42036–40.
17. Xu YN, Xia XX, Zhong JJ. Induction of ganoderic acid biosynthesis by Mn^{2+} in static liquid cultivation of *Ganoderma lucidum*. Biotechnol Bioeng. 2014;111:2358–65.
18. Hernández-Ortiz P, Espeso EA. Phospho-regulation and nucleocytoplasmic trafficking of CrzA in response to calcium and alkaline-pH stress in *Aspergillus nidulans*. Mol Microbiol. 2013;89:532–51.
19. Hernández-Ortiz P, Espeso EA. Spatiotemporal dynamics of the calcineurin target CrzA. Cell Signal. 2017;29:168–80.
20. Culotta VC, Yang M, Hall MD. Manganese transport and trafficking: lessons learned from *Saccharomyces cerevisiae*. Eukaryot Cell. 2005;4:1159–65.
21. Huang XJ, Shin JH, Pinochet-Barros A, Su TT, Helmann JD. *Bacillus subtilis* MntR coordinates the transcriptional regulation of manganese uptake and efflux systems. Mol Microbiol. 2017;103:253–68.
22. Luk E, Jensen LT, Culotta VC. The many highways for intracellular trafficking of metals. J Biol Inorg Chem. 2003;8:803–9.
23. Pittman JK. Managing the manganese: molecular mechanisms of manganese transport and homeostasis. New Phytol. 2005;167:733–42.
24. Mandal D, Woolf TB, Rao R. Manganese selectivity of Pmr1, the yeast secretory pathway ion pump, is defined by residue Gln⁷⁸³ in transmembrane segment 6. Residue Asp⁷⁷⁸ is essential for cation transport. J Biol Chem. 2000;275:23933–8.
25. Ofiteru AM, Ruta LL, Rotaru C, Dumitru I, Ene CD, Neagoe A, Farcasanu IC. Overexpression of the *PHO84* gene causes heavy metal accumulation and induces Ire1p-dependent unfolded protein response in *Saccharomyces cerevisiae* cells. Appl Microbiol Biotechnol. 2012;94:425–35.
26. Antebi A, Fink GR. The yeast Ca^{2+} -ATPase homologue, PMR1, is required for normal Golgi function and localizes in a novel Golgi-like distribution. Mol Biol Cell. 1992;3:633–54.
27. Mach-Aigner AR, Pucher ME, Steiger MG, Bauer GE, Preis SJ, Mach RL. Transcriptional regulation of *xyl1*, encoding the main regulator of the xylanolytic and cellulolytic enzyme system in *Hypocrea jecorina*. Appl Environ Microb. 2008;74:6554–62.
28. Takahashi A, Camacho P, Lechleiter JD, Herman B. Measurement of intracellular calcium. Physiol Rev. 1999;79:1089–125.
29. Xu YN, Xia XX, Zhong JJ. Induced effect of Na plus on ganoderic acid biosynthesis in static liquid culture of *Ganoderma lucidum* via calcineurin signal transduction. Biotechnol Bioeng. 2013;110:1913–23.
30. Feske S, Rao A, Hogan PG. The Ca^{2+} -calcineurin-NFAT signalling pathway. In: Krebs J, Michalak M, editors. New comprehensive biochemistry. Calcium: a matter of life or death. New York: Elsevier; 2007. p. 365–401.
31. Martinez D, Berka RM, Henrissat B, Saloheimo M, Arvas M, Baker SE, Chapman J, Chertkov O, Coutinho PM, Cullen D, et al. Genome sequencing and analysis of the biomass-degrading fungus *Trichoderma reesei* (syn. *Hypocrea jecorina*). Nat Biotechnol. 2008;26:553–60.
32. Lang RJ, Hashitani H, Tonta MA, Suzuki H, Parkington HC. Role of Ca^{2+} entry and Ca^{2+} stores in atypical smooth muscle cell autorhythmicity in the mouse renal pelvis. Br J Pharmacol. 2007;152:1248–59.
33. Bowman BJ, Abreu S, Johl JK, Bowman EJ. The *pmr* gene, encoding a Ca^{2+} -ATPase, is required for calcium and manganese homeostasis and normal development of hyphae and conidia in *Neurospora crassa*. Eukaryot Cell. 2012;11:1362–70.
34. Dürr G, Strayle J, Plemper R, Elbs S, Klee SK, Catty P, Wolf DH, Rudolph HK. The medial-Golgi ion pump Pmr1 supplies the yeast secretory pathway with Ca^{2+} and Mn^{2+} required for glycosylation, sorting, and endoplasmic reticulum-associated protein degradation. Mol Biol Cell. 1998;9:1149–62.
35. Maeda T, Sugijara R, Kita A, Saito M, Deng L, He Y, Yabin L, Fujita Y, Takegawa K, Shuntoh H, et al. Pmr1, a P-type ATPase, and Pdt1, an *Nramp* homologue, cooperatively regulate cell morphogenesis in fission yeast: the importance of Mn^{2+} homeostasis. Genes Cells. 2004;9:71–82.
36. Mandal D, Rulli SJ, Rao R. Packing interactions between transmembrane helices alter ion selectivity of the yeast Golgi Ca^{2+} / Mn^{2+} -ATPase PMR1. J Biol Chem. 2003;278:35292–8.
37. Paraszkievicz K, Frycie A, Slaba M, Dlugonski J. Enhancement of emulsifier production by *Curvularia lunata* in cadmium, zinc and lead presence. Biometals. 2007;20:797–805.
38. Xu YN, Zhong JJ. Impacts of calcium signal transduction on the fermentation production of antitumor ganoderic acids by medicinal mushroom *Ganoderma lucidum*. Biotechnol Adv. 2012;30:1301–8.
39. Jakubovics NS, Jenkinson HF. Out of the iron age: new insights into the critical role of manganese homeostasis in bacteria. Microbiol. 2001;147:1709–18.
40. Ouyang ZM, He M, Oman T, Yang XF, Norgard MV. A manganese transporter, BB0219 (BmtA), is required for virulence by the Lyme disease spirochete, *Borrelia burgdorferi*. Proc Natl Acad Sci USA. 2009;106:3449–54.
41. Peris-Peris C, Serra-Cardona A, Sánchez-Sanuy F, Campo S, Ariño J, San Segundo B. Two NRAMP6 isoforms function as iron and manganese transporters and contribute to disease resistance in Rice. Mol Plant Microbe. 2017;30:385–98.
42. Rosch JW, Gao G, Ridout G, Wang YD, Tuomanen EI. Role of the manganese efflux system *mntE* for signalling and pathogenesis in *Streptococcus pneumoniae*. Mol Microbiol. 2009;72:12–25.
43. Cohen A, Nelson H, Nelson N. The family of SMF metal ion transporters in yeast cells. J Biol Chem. 2000;275:33388–94.
44. Luk EEC, Culotta VC. Manganese superoxide dismutase in *Saccharomyces cerevisiae* acquires its metal co-factor through a pathway involving the *Nramp* metal transporter, *Smf2p*. J Biol Chem. 2001;276:47556–62.
45. Wykoff DD, O'Shea EK. Phosphate transport and sensing in *Saccharomyces cerevisiae*. Genetics. 2001;159:1491–9.
46. Dancis A, Haile D, Yuan DS, Klausner RD. The *Saccharomyces cerevisiae* copper transport protein (Ctr1p). Biochemical characterization, regulation by copper, and physiologic role in copper uptake. J Biol Chem. 1994;269:25660–7.
47. Dix DR, Bridgham JT, Broderius MA, Byersdorfer CA, Eide DJ. The *FET4* gene encodes the low affinity Fe(II) transport protein of *Saccharomyces cerevisiae*. J Biol Chem. 1994;269:26092–9.
48. Hassett R, Dix DR, Eide DJ, Kosman DJ. The Fe(II) permease Fet4p functions as a low affinity copper transporter and supports normal copper trafficking in *Saccharomyces cerevisiae*. Biochem J. 2000;351:477–84.
49. Zhao H, Eide D. The *ZRT2* gene encodes the low affinity zinc transporter in *Saccharomyces cerevisiae*. J Biol Chem. 1996;271:23203–10.
50. Zhao H, Eide D. The yeast *ZRT1* gene encodes the zinc transporter protein of a high-affinity uptake system induced by zinc limitation. Proc Natl Acad Sci USA. 1996;93:2454–8.

51. Ariño J, Ramos J, Sychrová H. Alkali metal cation transport and homeostasis in yeasts. *Microbiol Mol Biol Rev.* 2010;74:95–120.
52. Thewes S. Calcineurin–Crz1 signaling in lower eukaryotes. *Eukaryot Cell.* 2014;13:694–705.
53. Saidi Y, Finka A, Goloubinoff P. Heat perception and signalling in plants: a tortuous path to thermotolerance. *New Phytol.* 2011;190:556–65.
54. Wang H, Liang Y, Zhang B, Zheng W, Xing L, Li M. Alkaline stress triggers an immediate calcium fluctuation in *Candida albicans* mediated by Rim101p and Crz1p transcription factors. *FEMS Yeast Res.* 2011;11:430–9.
55. Michielse CB, Hooykaas PJJ, van der Hondel CAMJJ, Ram AFJ. *Agrobacterium*-mediated transformation of the filamentous fungus *Aspergillus awamori*. *Nat Protoc.* 2008;3:1671–8.
56. Mandels M, Weber J. The production of cellulases. Cellulases and their applications. Washington, DC: American Chemical Society; 1969. p. 391–414.
57. Wang MY, Zhao QS, Yang JH, Jiang BJ, Wang FZ, Liu KM, Fang X. A mitogen-activated protein kinase Tmk3 participates in high osmolarity resistance, cell wall integrity maintenance and cellulase production regulation in *Trichoderma reesei*. *PLoS ONE.* 2013;8:e72189.
58. Bischof R, Fourtis L, Limbeck A, Gamauf C, Seiboth B, Kubicek CP. Comparative analysis of the *Trichoderma reesei* transcriptome during growth on the cellulase inducing substrates wheat straw and lactose. *Biotechnol Biofuels.* 2013;6:127.
59. Zhang G, Liu P, Wei W, Wang X, Wei D, Wang W. A light-switchable bidirectional expression system in filamentous fungus *Trichoderma reesei*. *J Biotechnol.* 2016;240:85–93.
60. Steiger MG, Mach RL, Mach-Aigner AR. An accurate normalization strategy for RT-qPCR in *Hypocrea jecorina* (*Trichoderma reesei*). *J Biotechnol.* 2010;145:30–7.
61. Zhang L, Zhao X, Zhang G, Zhang J, Wang X, Zhang S, Wang W, Wei D. Light-inducible genetic engineering and control of non-homologous end-joining in industrial eukaryotic microorganisms: LML 3.0 and OFN 1.0. *Sci Rep.* 2016;6:20761.

Submit your next manuscript to BioMed Central and we will help you at every step:

- We accept pre-submission inquiries
- Our selector tool helps you to find the most relevant journal
- We provide round the clock customer support
- Convenient online submission
- Thorough peer review
- Inclusion in PubMed and all major indexing services
- Maximum visibility for your research

Submit your manuscript at
www.biomedcentral.com/submit

